AUTOMATIC DESIGN OF ORIGAMIC ARCHITECTURE PAPER POP-UPS

LE NGOC SANG

NATIONAL UNIVERSITY OF SINGAPORE

2013

AUTOMATIC DESIGN OF ORIGAMIC ARCHITECTURE PAPER POP-UPS

LE NGOC SANG

B.Sc. (Hons.), NUS

A THESIS SUBMITTED FOR THE DEGREE OF

DOCTOR OF PHILOSOPHY

DEPARTMENT OF COMPUTER SCIENCE
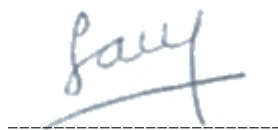
NATIONAL UNIVERSITY OF SINGAPORE

2013

To my parents, my wife and my little daughter

Declaration

I hereby declare that this thesis is my original work and it has been written by me in its entirety.

I have duly acknowledged all the sources of information which have been used in the thesis.

This thesis has also not been submitted for any degree in any university previously.

Le Ngoc Sang

30 April 2013

Acknowledgements

I am deeply grateful to Dr. Low Kok-Lim, my Ph.D. supervisor, for his patient guidance, continued encouragement and constant support. He always shares with me insightful advice, while giving me sufficient room to grow. His wisdom, kindness, and wonderful personality will always inspire me.

I would also like to thank Leow Su Jun, Le Nguyen Tuong Vu and Conrado Ruiz Jr. for their prior work and consistent help in this research. I really enjoy working with them.

Many thanks to Drs. Tan Tiow Seng, Cheng Ho-lun, Lee Yong Tsui and Leong Hon Wai for their valuable feedback and suggestions on my thesis. Thanks to the members of the graphics and geometry group for their interesting discussions and sharings during our weekly meetings. I can never forget my wonderful work environment in G^3 lab and especially NUS, my second home.

I reserve the last words of thanks for my family, for their many years of love, support and encouragement. I am lucky to have met and married my wife, who has always been by my side during the last and toughest years of my Ph.D. program. This thesis is dedicated to my parents, my wife and my lovely little daughter.

Contents

Summary

Origamic architecture (OA) is a paper art form that involves cutting and folding a single piece of paper to resemble three-dimensional objects. Because of the geometric and physical constraints, OA design is labor-intensive and requires considerable skills. While similar to pop-up books, OA is created with no gluing, which puts additional constraints to the design process.

A number of computer tools have been developed to assist the OA design process. However, in these tools, the user still needs to manually determine where and how the cuts and folds should be positioned. Automatic design of OA has not been well-studied.

In this thesis, we present an algorithm for automatic design of an OA that closely depicts an input 3D model. Our algorithm is grounded on a general set of geometric conditions to ensure the stability and foldability of the pop-ups. The generality of the conditions allows our algorithm to generate valid structures that were excluded by previous algorithms. Moreover, our method uses an image-domain approach that allows us to capture important shapes using image segmentation. Our algorithm is significantly better than the existing methods in the preservation of contours, surfaces and volume. The designs have also been shown to resemble those created by real artists.

In addition, we propose a simple yet effective approach for analyzing the physical strength of OA structures. Our physical formulation is based on Kirchhoff-Love theory of plate and Finite Difference Method. It allows our system to automatically detect and correct physically weak paper structures in real time.

By combining both aspects, we guarantee that our final OA designs are both geometrically valid and phyiscally strong.

List of Figures

List of Figures

List of Tables

List of Publications

[1] S. N. Le, S. J. Leow, T.-V. Le, and K.-L. Low. Surface and contour-preserving origamic architecture paper pop-ups. *IEEE Transactions on Visualization and Computer Graphics*, 20(2): 276–288, February 2014.

This publication contains the work on origamic architecture paper pop-up in Chapter 3.

[2] T.-V. Le, K.-L. Low, C. Ruiz Jr., and S. N. Le. Automatic paper slice-form design from 3d solid models. *IEEE Transactions on Visualization and Computer Graphics*, 19(11): 1795–1807, November 2013.

This publication partially contains a similar formulation to the geometric stability of paper pop-up in Chapter 3.

[3] C. J. Ruiz, S. N. Le, and K.-L. Low. Generating multi-style paper pop-up designs using 3d primitive fitting. In *ACM SIGGRAPH Asia Technical Briefs*, Hong Kong, 2013.

This publication partially contains the geometric formulation for the foldability of v-structure paper pop-up in Chapter 4.

[4] C. J. Ruiz, S. N. Le, J. Yu, and K.-L. Low. Multi-style paper pop-up designs from 3d models. *Computer Graphics Forum*, 3(2):, 2014.

This publication partially contains the geometric formulation for the foldability of multi-structure paper pop-up in Chapter 4.

Chapter 4

Origamic Architecture with Non-parallel Folds

In Chapter 3, we presented the theory and algorithm for the automatic design of traditional parallel origamic architecture. Although the formulated OAs only consisted of parallel fold lines, they were able to feature numerous types of 3D shapes, from architectural to organic objects.

However, we also observe that in practical OA design, artists occasionally use non-parallel folds (Fig 4.1). Since such folds are not constrained in a fixed orientation, they may be used to approximate slanted surfaces better. In addition, a non-parallel fold may sometimes be used to replace a series of parallel folds, which reduces the difficulty of the actual pop-up creation (Fig. 4.2).

Hence, in this chapter, we explore an extended solution for OA design that take into account both parallel and non-parallel folds. We

FIGURE 4.1: Pop-up designs with non-parallel folds.

investigate the conditions for geometrically valid OA with non-parallel folds, as well as an algorithm to generate such folds. For convenience, from this chapter, we will call an OA with only parallel folds, as described in Chapter 3, *parallel OA*, and an OA with non-parallel folds *general OA*. The work on general OA in this chapter has also been presented partially in [88, 89].

While non-parallel folds can be used to capture slanted surfaces, OA still mainly consist of parallel folds, because they create nicely uniform shadowing effects when popping up. Hence, we still use the algorithm described in Chapter 3 for parallel OA as the backbone for designing general OA. In this chapter, we will extend it to design non-parallel folds for suitable slanted surfaces. Note that we only reconstruct surfaces that are visible in the $45°$ orthographic view, because our abstraction method is applied in this view.

First, in order to describe the algorithm for non-parallel fold construction, we need to investigate the geometric conditions for its validity, including both foldability and stability.
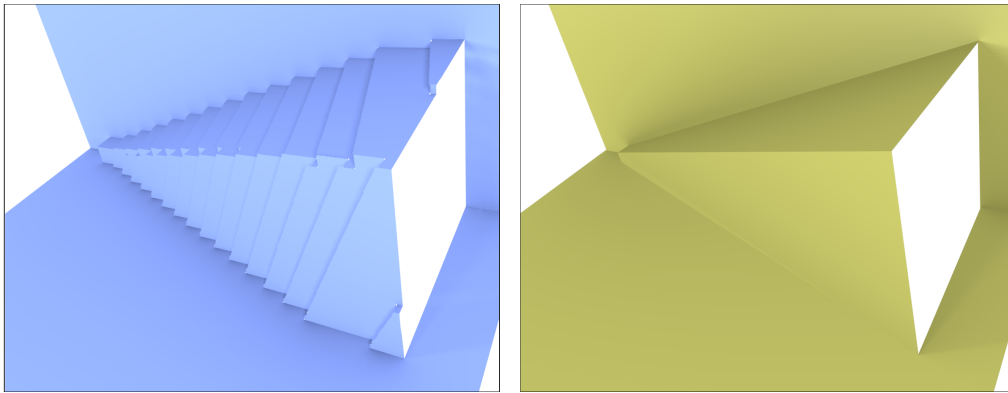
FIGURE 4.2: A series of parallel structures can be replaced by a single non-parallel one for easier cutting and folding.

4.1 Geometric Formulations

4.1.1 General OA Components

The components of a general OA are similar to those of a parallel OA defined in Section 3.1.1 on page 29, except that the fold lines do not need to be parallel to the central fold. In addition, we denote a popped-up structure that contains two patches connected by a non-parallel fold as a *v-structure*, since these two patches form a v-shape structure. To facilitate our further discussion, we distinguish between *concave folds* and *convex folds* (Fig. 4.3 (a)). We also call the fold line between the two patches that a popped-up structure is based on a *base fold line*, and the angles formed by this line and the two convex folds *base angles*. Note that when we handle an angle between two fold lines, we consider their extensions, not just the actual fold segments. This is because some *v*-structures may be cut off at their tips, as shown in Section 4.3 on the results.

In our study, we only consider the *v*-structures whose convex fold lines intersect along the base fold line. This is similar to the type of structures considered in [67] and [36]. Specifically, the concurrency of the fold lines gives the *v*-structure a potential to pop up. Additionally, in each *v*-structure, we assume the angles between its convex and concave fold lines to be smaller than $90°$. Otherwise, they form a straight line and two patches of the structure may rotate freely when it is open at $180°$ (Fig 4.3 (b)).

The definition of a general OA plan inherit the properties of a parallel OA plan, which were described in Definition 3.3 on page 30. We add two more properties to incorporate non-parallel folds as follows.
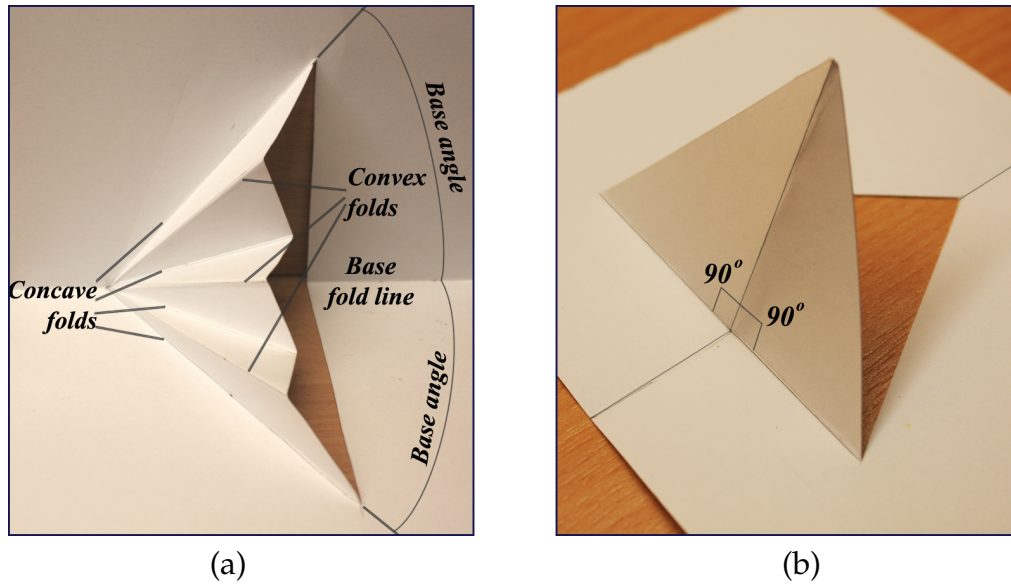
FIGURE 4.3: (a) The components in a v-structure. (b) A v-structure with two $90°$ angles may rotate freely when opened at $180°$.

Definition 4.1. *A general OA plan is a set of patches where*

1. *All the patches are co-planar and form a rectangular domain with possible holes.*

2. *They are non-intersecting, except at their boundaries.*

3. *For every patch p, there exists a path traversing from the back patch p_B to the floor patch p_F and containing p.*

4. *For every v-structure, its concave fold line and convex fold lines intersect at one point along the base fold line.*

5. *For every v-structure, the inner angles between its convex fold line and concave fold lines are smaller than $90°$.*

General OA plans share the first 3 common properties with traditional parallel OA plan. Properties 4 and 5 correspond to the assumptions on v-structures described earlier.

4.1.2 Foldability of General OA

The foldability of a general OA is defined similarly to that of a parallel OA, which means the OA plan needs to be foldable from $\theta = 180°$ to $\theta = \epsilon$ without affecting the shapes, pairwise adjacency and non-intersection of the patches.

In Proposition 3.1 on page 31, OA foldability is examined by projecting the popped-up structure onto the xz-plane and check whether it matches the OA plan. Such condition is useful for parallel OA design, because its abstraction utitilizes a $45°$ orthographic projection.

However, non-parallel patches do not project onto the OA plan in one fixed direction. Hence, we may not re-use Proposition 3.1 for checking the foldability of a general OA. In this section, we present another set of foldability conditions for v-structures and general OA.

4.1.2.1 Foldability of a Path of v-Structures

First, we consider an OA plan that only consists of a series of n v-structures forming a $2n$-path between two bases p_1 and p_2. For convenience, we call this series a v-path. Let us denote the outermost base angles as ω_α and ω_β. The angles between alternating convex and concave fold lines on the v-structures are denoted as α_1, β_1, α_2, β_2, ..., α_n, β_n. We now present an angle condition for the foldability of a v-path.

Proposition 4.1. *An OA plan consisting of only a path of n v-structures is foldable if and only if $\omega_\alpha = \beta_1 + \beta_2 + ... + \beta_n$, and $\omega_\beta = \alpha_1 + \alpha_2 + ... + \alpha_n$.*

An illustration of Proposition 4.1 is shown in Fig. 4.4. The necessity of this proposition for a single v-structure has been described in some
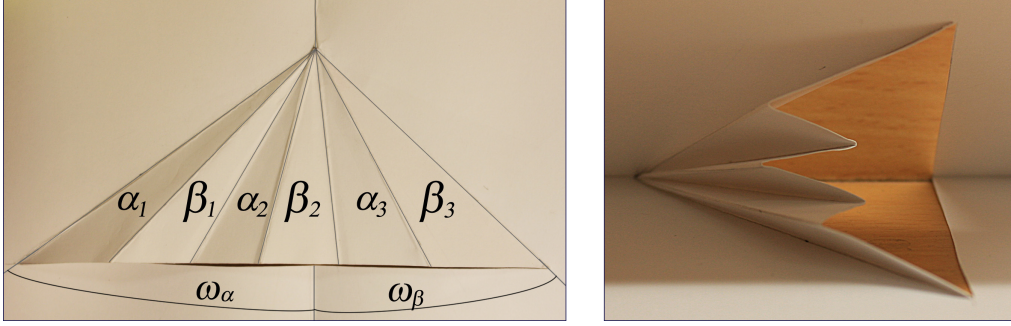
FIGURE 4.4: A foldable path of v-structures and its angles.

previous studies, such as [67] and [36]. In this section, we prove the sufficiency and necessity of this proposition for multiple v-structures.

Proof.

Sufficiency. Assume that we have an OA plan of n v-structures satisfying $\omega_\alpha = \beta_1 + \beta_2 + ... + \beta_n$, and $\omega_\beta = \alpha_1 + \alpha_2 + ... + \alpha_n$, which lead to $\omega_\alpha + \alpha_1 - \beta_1 + ... + \alpha_n - \beta_n - \omega_\beta = 0$. We will show that this OA is fully foldable.

First, consider an OA plan consisting of only one v-structure. If $\omega_{\alpha_0} + \alpha_0 - \beta_0 - \omega_{\beta_0} = 0$, then it is possible to put the OA in the fully closed configuration (Fig. 4.5 (a)). Now we can also prove that the OA is foldable to any other opening angle. As shown in Fig. 4.5 (b), when the back patch is rotated, point P remains the intersection of three spheres centered at O, O_α and O_β, with radii OP, $O_\alpha P$ $O_\beta P$, respectively. This intersection can always be found at any arbitrary opening angle, because $OO_\alpha < OP + O_\alpha P$ and $OO_\beta < OP + O_\beta P$.

To fold an OA with n v-structures, we can fold each of them successively. When we completely fold the first v-structure that is adjacent to the floor patch, the remaining $n - 1$ v-structures will form with the floor patch an angle $w_\alpha + \alpha_1 - \beta_1$. By continuing to fold completely each of the first $n - 1$ v-structures, the last v-structure will form with the floor patch an angle $w_\alpha + \alpha_1 - \beta_1 + ... + \alpha_{n-1} - \beta_{n-1}$. Since $\omega_\alpha + \alpha_1 - \beta_1 + ... + \alpha_n - \beta_n -$
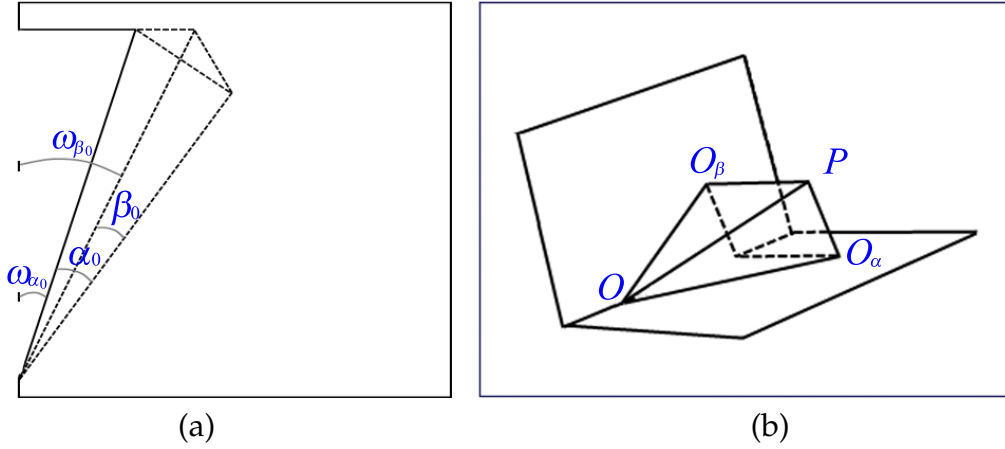
FIGURE 4.5: (a) A v-structure in its closed configuration illustrates the relationship between its angles. (b) The points in a v-structure when it is opened.

$\omega_\beta = 0$, the last v-structure satisfies the foldable condition for a single v-structure, $\omega_{\alpha_0} + \alpha_0 - \beta_0 - \omega_{\beta_0} = 0$, where $\omega_{\alpha_0} = w_\alpha + \alpha_1 - \beta_1 + ... + \alpha_{n-1} - \beta_{n-1}$, $\omega_{\beta_0} = \omega_\beta$, $\alpha_0 = \alpha_n$ and $\beta_0 = \beta_n$. Hence, the OA is fully foldable.

Necessity. Assume that we have a foldable OA plan consisting of n v-structures. We will show that their angles satisfy $\omega_\alpha = \beta_1 + \beta_2 + ... + \beta_n$, and $\omega_\beta = \alpha_1 + \alpha_2 + ... + \alpha_n$.

When it is fully closed, as shown in Fig. 4.5 (a), we have $\omega_\alpha + \alpha_1 - \beta_1 + \alpha_2 - \beta_2 + ... - \omega_\beta = 0$, which means $\omega_\alpha + \alpha_1 + \alpha_2 + ... + \alpha_n = \omega_\beta + \beta_1 + \beta_2 + ... + \beta_n$. On the other hand, when the OA plan is opened flat, we also have $\omega_\alpha + \omega_\beta = \alpha_1 + \beta_1 + \alpha_2 + \beta_2 + ... + \alpha_n + \beta_n$ (Fig. 4.4). Hence, $\omega_\alpha = \beta_1 + \beta_2 + ... + \beta_n$, and $\omega_\beta = \alpha_1 + \alpha_2 + ... + \alpha_n$. $\qquad\square$

Our generalization from a single v-structure to multiple v-structures allows more complex OA. However, the foldability of v-structures is not the only consideration in the design. We also need to guarantee that different structures do not overlap or intersect during the opening and closing process.

4.1.2.2 Foldability of a Combination of Structures

When there are only parallel fold lines, as discussed in Chapter 3, no inter-structure overlapping occurs, since the projections of all the points in the pop-up along the central fold are fixed. In addition, the patches always remain parallel to the two outermost bases and do not intersect, except along the fold lines. Fig. 4.6 (a) shows the coverage of a parallel structure at $180°$ and $0°$ opening angles.

(a)   (b)
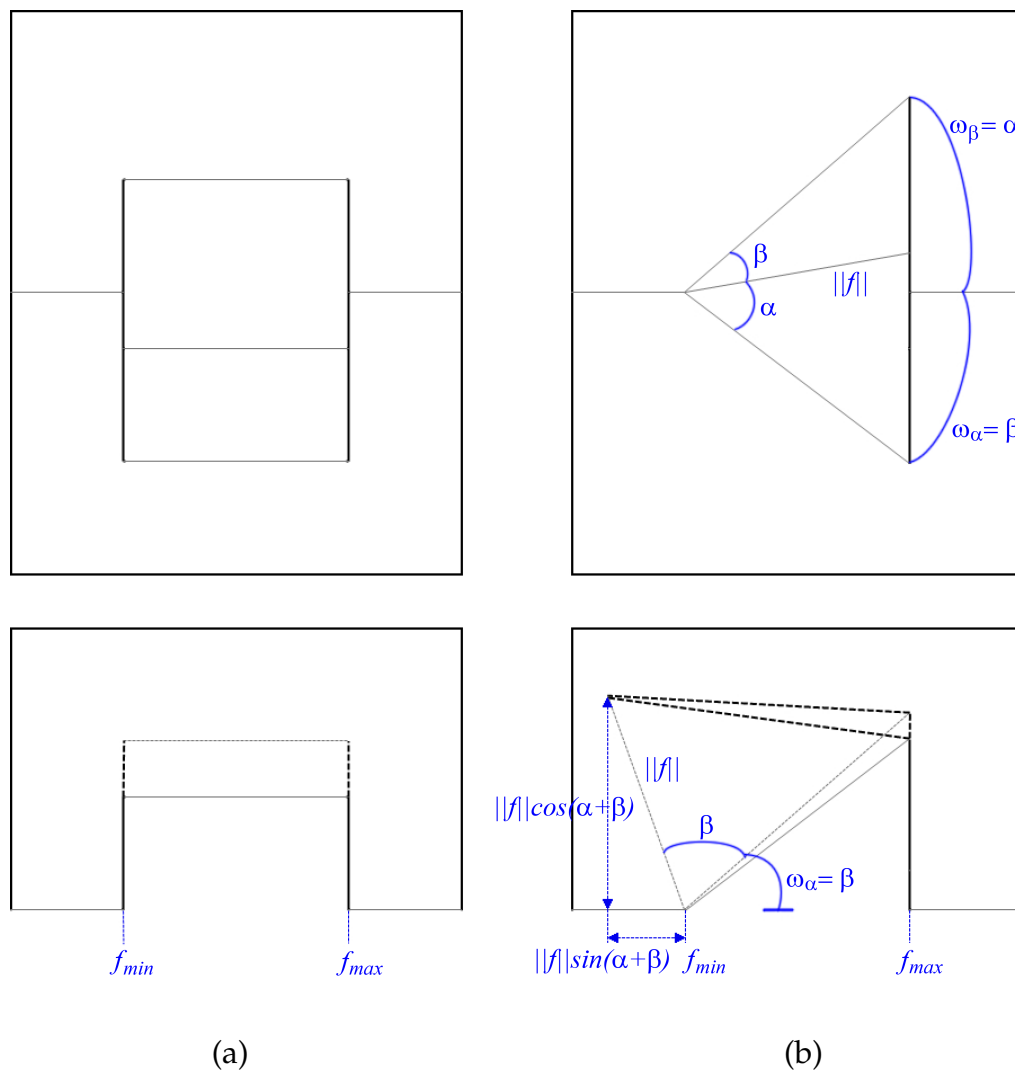
FIGURE 4.6: (a) OA plan of a parallel structure (top) and its coverage when fully closed (bottom). (b) OA plan of a v-structure (top) and its coverage when fully closed (bottom).

On the other hand, when a v-structure is used, its projection on the base fold line move during the opening and closing process. We need to compute the range of movement of a v-structure to avoid inter-structure overlapping.

Consider a v-structure whose fold lines form two angles α and β, as shown in Fig. 4.6 (b, top). In order for the structure to be foldable, α, β, and the base angles ω_α, ω_β must satisfy $\omega_\alpha = \beta$ and $\omega_\beta = \alpha$.

If the fold lines of the v-structure intersect at f_{min} along the base fold, and its projection lie from f_{min} to f_{max} at $180°$ opening angle, then the actual length of its convex fold line is $\|f\| = (f_{max} - f_{min})/cos(\gamma)$, where $|\gamma| = |\beta - \omega_\alpha| = |\alpha - \omega_\beta| = |\beta - \alpha|$. Then at $0°$ angle, the projection of this convex fold line on the base fold has length $\|f\|cos(\alpha + \beta)$. Additionally, its projection on the axis perpendicular to the base fold has length $\|f\|sin(\alpha + \beta)$.

Hence, at $0°$ opening angle, the v-structure lies within $[f_{min} - (f_{max} - f_{min})cos(\alpha + \beta)/cos(\alpha - \beta), f_{max}]$ along the base fold, and $[0, (f_{max} - f_{min})sin(\alpha + \beta)/cos(\alpha - \beta)]$ along its perpendicular axis Fig. 4.6 (b, bottom).

Knowing the coverage of each structure when folded from $180°$ to $0°$, we present the conditions for the foldability of a general OA plan as follows.

Proposition 4.2. *A general OA plan is foldable if it satisfies*

1. *All v-structures satisfy the angle condition in Proposition 4.1.*

2. *No parallel structure is based on a v-structure.*

3. *For each base fold line, there is no overlapping between the coverages of structures lying on it when they are folded.*

The first condition follows Proposition 4.1. The second condition is required for every parallel structure to pop up, because its convex fold line has to be always parallel to the base fold. Finally, the third condition is based on the coverage calculation earlier.

4.1.3   Stability of General OA

The stability of a general OA is defined similarly to Definition 3.4 on page 33 for a parallel OA. In brief, it needs to be able to fully pop up when the user turns only the back and floor patches, but not any other patch.

As discussed in Section 3.1.3 on page 33, previous studies only considered 1-paths and 2-paths for stable parallel OAs. Similarly, they consider only 2-paths for stable v-structures. This may greatly limit the possibility for designing v-structures, especially when we have proven in Section 4.1.2 that an arbitrary path of v-structures is foldable, as long as it satifies the angle condition.

In Section 3.2.4 on page 53, parallel structures can be made stable by creating double connections. We observe that an equivalent approach can also be used for v-structures. However, since the fold lines and patches in v-structures are not parallel, we define double connections slightly differently and based on the angles between the fold lines.

Definition 4.2. *Consider 4 mutually non-coplanar patches p_1, p_2, p_3, p_4, where p_1 and p_2 intersect p_3 and p_4 at l_{13}, l_{14}, l_{23}, and l_{24}, respectively. The angles between (l_{13}, l_{14}), (l_{23}, l_{24}), (l_{13}, l_{23}) and (l_{14}, l_{24}) are denoted as $\delta_{34/1}$, $\delta_{34/2}$, $\delta_{12/3}$ and $\delta_{12/4}$. We say (p_1, p_2) and (p_3, p_4) are* doubly-connected *if $\delta_{34/1} = \delta_{34/2}$ and $\delta_{12/3} = \delta_{12/4}$. In such case, the structure (p_1, p_2, p_3, p_4) is also called a* double connection.
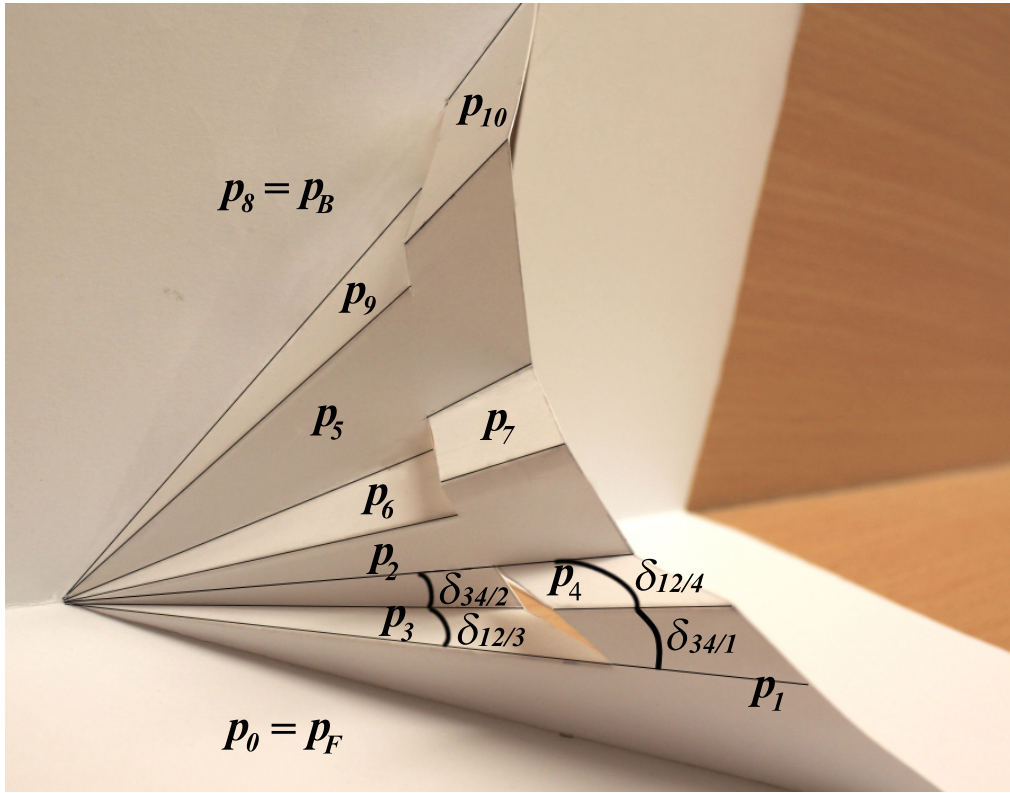
FIGURE 4.7: Three doubly connected v-structures (p_1, p_2, p_3, p_4), (p_2, p_5, p_6, p_7) and (p_5, p_8, p_9, p_{10}), as described in Definition 4.2. For instance, in the first double connection, we have $\delta_{34/1} = \delta_{34/2}$ and $\delta_{12/3} = \delta_{12/4}$.

Fig. 4.7 illustrates double connections of v-structures. We utilize this type of connection to introduce a new stability condition for a path of v-structures.

Proposition 4.3. *A path of v-structre is foldable and stable if all pairs of even (odd) patches along the path are doubly connected.*

The odd and even patches are defined similarly to Section 3.1.3 on page 33. If $\mathbb{P} = \{p_0 = p_B, p_1, \ldots, p_n, p_{n+1} = p_F\}$ be a path traversing from the back patch to the floor patch, then along $\mathbb{P}$, p_{2k} is called an even patch and p_{2k+1} is called an odd patch, where $0 \leq k \leq \lfloor n/2 \rfloor$.

A sample foldable and stable path as described in Proposition 4.3 is shown in Fig. 4.7. The stability conditions for parallel structures and v-structures are analogous. However, while the foldability of parallel

double connection is intuitive due to parallelism, that of non-parallel double connection is not straightforward. We prove the foldability of doubly-connected v-structures as follows.
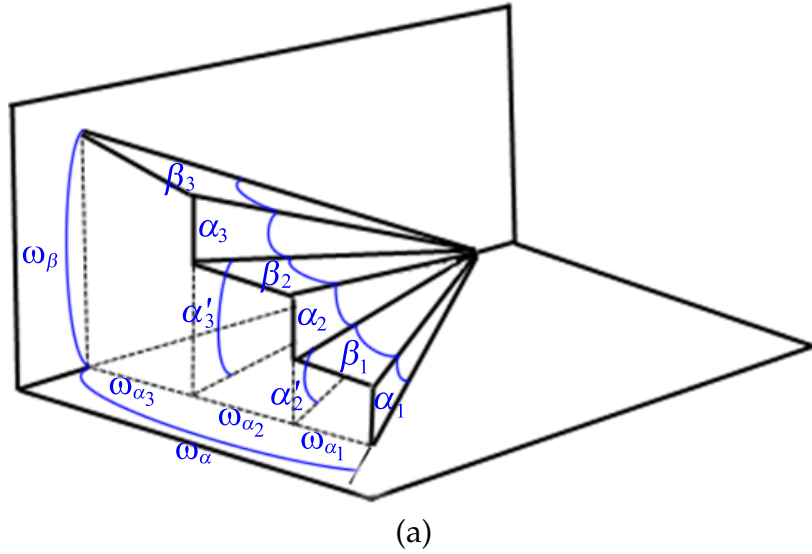
(a)
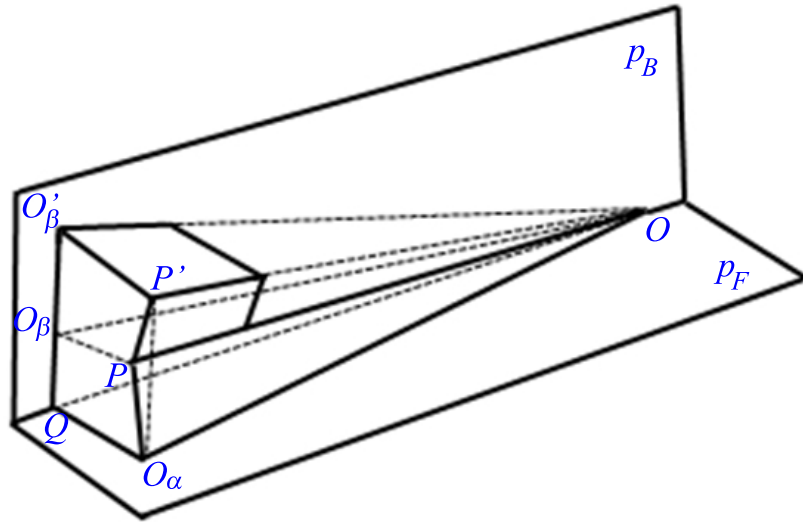
(b)

FIGURE 4.8: (a) A path of n v-structures can be considered a combination of n single v-structures based on the floor patch. (b) Extra patches can be added to a single v-structure to form a foldable, doubly-connected v-structure.

Proof.

Consider a foldable OA consisting of only a v-path. As shown in Fig. 4.8 (a), at any opening angle, we can hold the patches so that the intersections of their extensions with the base patches satisfy $\omega_{\alpha_i} = \beta_i$ for

all $i \in [1, n]$, $\omega_\beta = \alpha_n + \alpha_n'$, and $\alpha_{i+1}' = \alpha_i + \alpha_i'$ for all $i \in [1, n-1]$. This is possible because $\omega_\alpha = \sum_1^n \beta_i$, and $\omega_\beta = \sum_1^n \alpha_i$.

Hence, the OA can be treated as a vertical accumulation of n simple OAs, each consisting of only one foldable v-structure. In order to show that the doubly-connected v-path is foldable, now we only need to show that doubly connecting each foldable v-structure still allows it to fold completely.

Consider a foldable v-structure containing patches p_B, p_F, $OO_\alpha P$ and $OO_\beta P$ (Fig. 4.8 (b)). We add patches OPP' and $OP'O_\beta'$ on top of this v-structure such that $\widehat{POP'} = \widehat{O_\beta OO_\beta'}$ and $\widehat{POO_\beta} = \widehat{P'OO_\beta'}$. By Proposition 4.1, the v-structure $(OO_\beta P, p_B, OPP', OP'O_\beta')$ is also foldable, making the structure $(p_B, p_F, OO_\alpha P', OP'O_\beta')$ foldable and leading to $\widehat{O_\alpha OP'} = \widehat{QOO_\beta'}$. Note that we also have $\widehat{QOO_\beta'} = \widehat{QOO_\beta} + \widehat{O_\beta OO_\beta'} = \widehat{O_\alpha OP} + \widehat{POP'}$. Hence, $\widehat{O_\alpha OP'} = \widehat{O_\alpha OP} + \widehat{POP'}$. In other words, three patches $O_\alpha OP$, $O_\alpha OP'$ and POP' are co-planar. Hence, the resulting structure is a foldable doubly-connected v-structure, according to Definition 4.2.

$\square$

Besides the foldability of doubly-connected v-structures, we also examine its stability by using both simulated models and actual paper pop-ups. We create a number of OAs consisting of up to 5 v-structures. The angles between the fold lines are randomized such that they satisfy Proposition 4.1 and Definition 4.2.

Figs. 4.9 and 4.10 show a simulated model and an actual paper pop-up that make use of double connections to create foldable and stable v-structures. The simulation is done using V-REP software [24] and rendered with OpenGL. We observe that no patch is stuck or collapses,

81
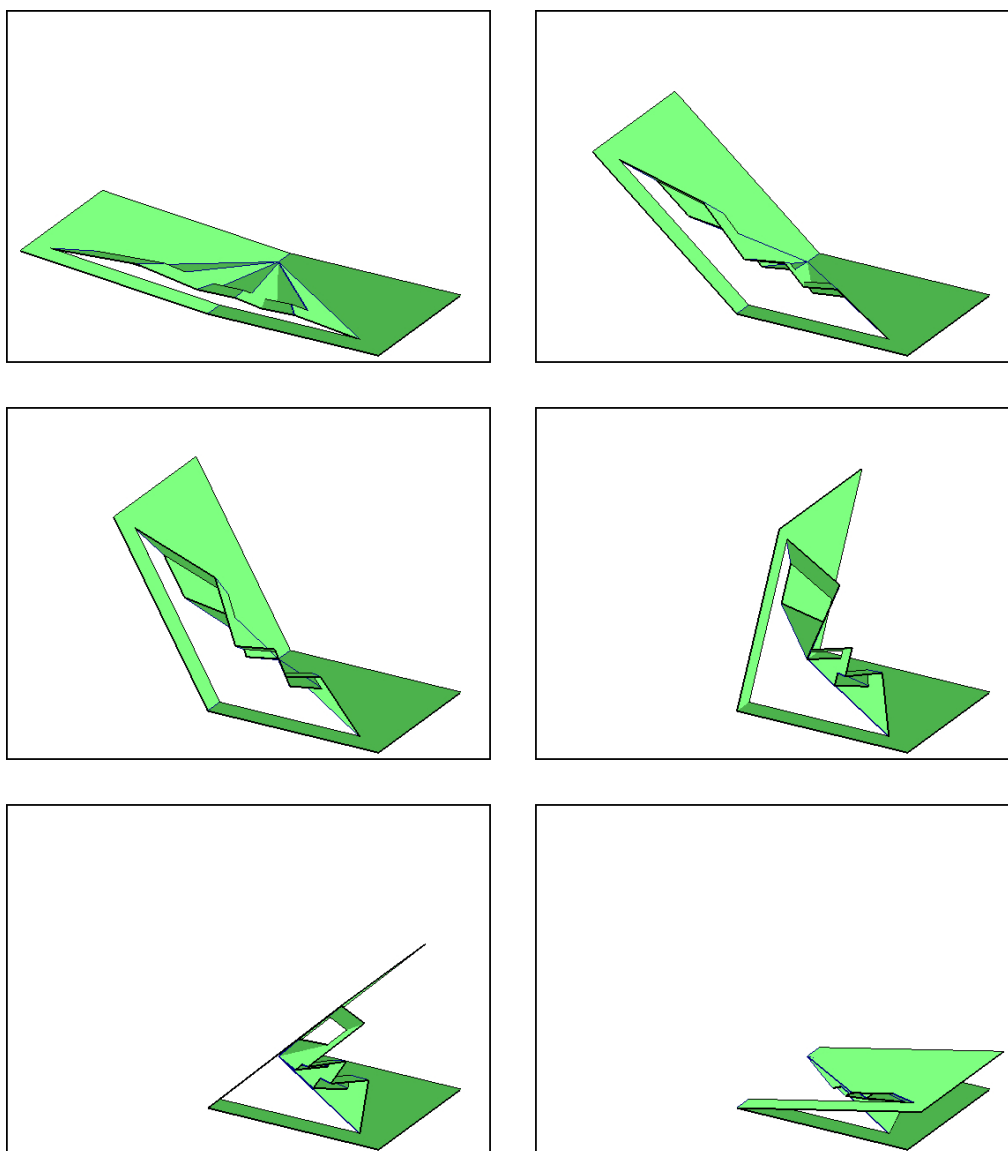
FIGURE 4.9: A simulated OA containing a path of 3 doubly connected v-structures. The closing motion of the OA is captured from top to bottom and left to right.

and all the patches move in a stable manner when we hold and turn only the two outermost patches.

Our experiments with both simulated and actual pop-ups empirically show the stability of doubly-connected v-structures. It is also observable that, for every doubly-connected v-structure, the possible orientation of each patch is constrained by that of the opposite patch. In a
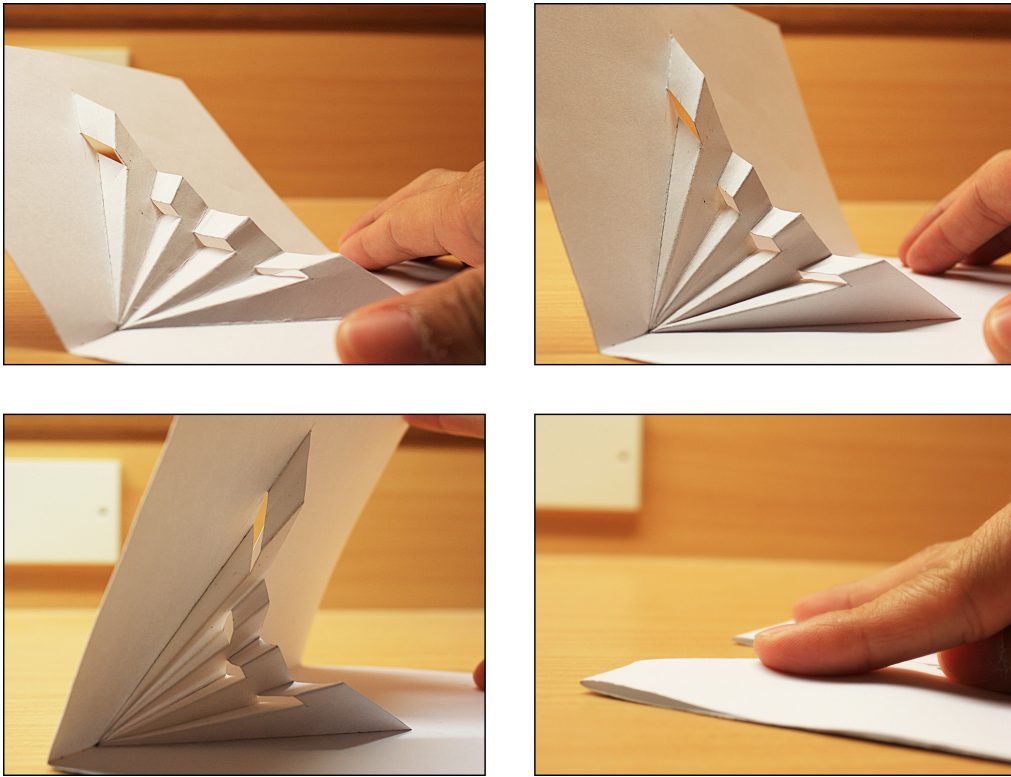
FIGURE 4.10: A real OA paper pop-up containing a path of 4 doubly connected v-structures.

v-path that consists of doubly-connected patches, their orientations are mutually constrained. Together with the positional constraints of the first and last patches, it may be possible to formulate a mathematical proof for the stability of doubly-connected v-structure.

Presently, such formal proof has yet been achieved. The main challenge is to find an appropriate relationship between the patches, the fold lines, or the points on the fold lines, such that it remains unchanged during the opening and closing of the v-structures. Earlier, for parallel OA, the parallelism between the patches holds true at any opening angle and guarantees their stability. An equivalent property is difficult to find for non-parallel folds. In particular, the points on the fold lines move along non-coplanar and non-parallel circles (Fig. 4.11). As a result, the orientations of the vectors connecting these points vary in a complex manner,
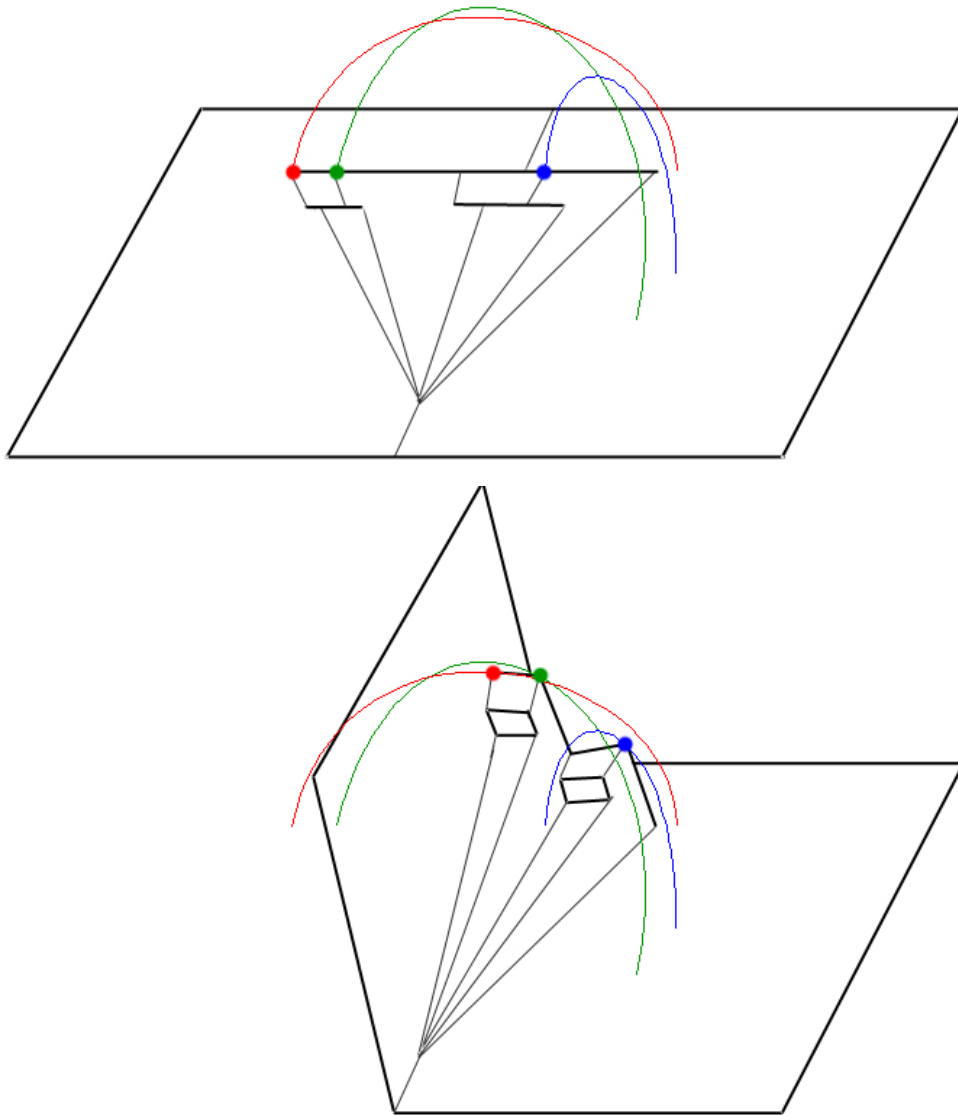
FIGURE 4.11: The points on a line in a non-parallel OA plan (top) will move along non-coplanar and non-parallel circles during the opening and closing process (bottom).

and investigating the constraints between them is not trivial.

Based on the empirical results, in this work, we use double connections as a means to stabilize paths of v-structures. We discuss our algorithm for designing general OAs that contain v-structures in the next section.

4.2   General OA Design Algorithm

We presented our algorithm for designing parallel origamic architecture in Section 3.2 on page 43. In order to design a general OA containing non-parallel structures, we extend that algorithm to create v-structures for appropriate slanted regions, instead of using parallel structures for all regions.

As described in Section 3.2.1 on page 45, the input surface is divided into distinct non-overlapping, smooth segments before patch generation. This pre-processing step is still performed for general OA design.

In our pipeline, the generation of v-structures is done after the surface segmentation and before the generation of parallel patches. By designing the OA in this order, we do not need to construct multiple parallel patches for a slanted surface if simpler v-structures can be used.

The design of v-structures starts with the surface segments produced from the pre-processing step. It then follows three main steps.

1. **Finding the potential surface segments that can be approximated using v-structures:** We select a list of surface segments that are potential for v-structure construction based on property 5 of Definition 4.1 on general OA plans, and conditions 2 and 3 of Proposition 4.2 on general OA foldability. More details are described in Section 4.2.1.

2. **Constructing foldable v-structures from the selected surface segments:** We compute the angles of the v-structures so that they approximate the selected surface segments closely, while satisfying property 4 of Definition 4.1, Proposition 4.1 and condition 1 of Proposition 4.2. We separate this step from the segment selection as

it requires exact calculation of the angles between the folds. More details are described in Section 4.2.2.

3. **Stabilizing v-structures:** We generate extra patches to form double connections, which are used to support the stability of v-structures, according to Proposition 4.3. More details are described in Section 4.2.3.

As the generation of non-parallel structures is a component of a unified pipeline for general OA design, in this algorithm, we still process the input surface using a $45°$ orthoggraphic view. V-structures are only generated for appropriate surface segments that are visible in this view. The details of our v-structure generation are described in the following subsections.

4.2.1 Potential Surface Segments for V-Structure Generation

Since each v-structure contains only two patches sharing a straight fold line, to construct it we first need to detect straight boundaries between adjacent surface segments. Similar to the approach in Section 3.2.1 on page 45, the adjacency of the segments is examined by thresholding the changes in depth and normal values in the segments. Then straight boundaries between adjacent segments are detected using Canny edge operator [13] and Progressive Probabilistic Hough Transform [73] techniques. The segments containing only straight fold lines that are not parallel to the base patches are marked for the next processing steps, which check whether the segments can be approximated using v-structures.

From the pairs of adjacent segments that share a straight boundary, we select those that do not have any two consecutive fold lines forming

(a)   (b)
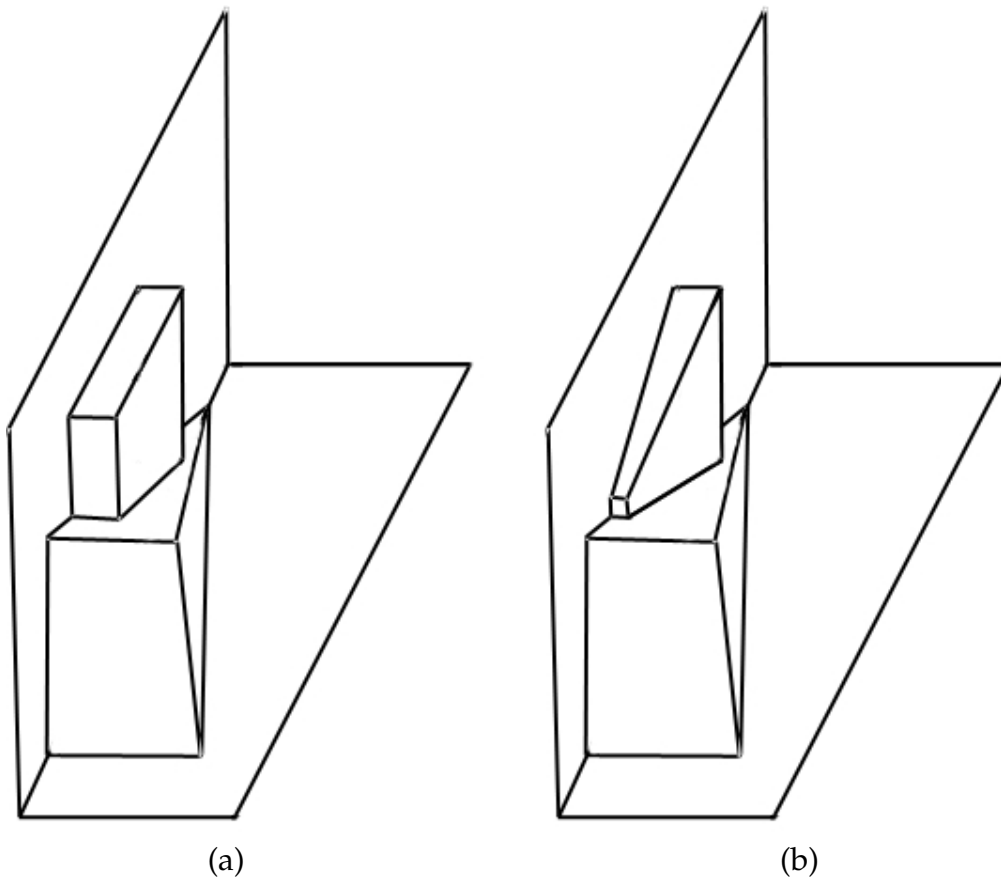
FIGURE 4.12: (a) A model with a parallel block basing on a non-parallel block is not a good candidate for v-structure generation, because the resulting OA will not be foldable. (b) A model with a non-parallel block basing on another one can still be converted into a foldable OA containing two foldable v-structures.

a $90°$ or larger angle. This criteria is to satisfy property 5 in Definition 4.1 (Fig. 4.3 (b)).

Next, we refine the list of selected segments so that they meet conditions 2 and 3 of Proposition 4.2. For condition 2, we remove from the list any non-base segment that is adjacent to another segment not potential for v-structure generation (Fig. 4.12 (a)). By doing this, we will not have any parallel structures basing on a v-structure. Note that the fold lines in a parallel structure need to be parallel to the base patches in

order for it to be foldable.

Finally, to fulfil condition 3 of Proposition 4.2, we compute the possible range of movement of the segments if the two outermost bases close fully at $0°$. This computation is based on section 4.1.2.2 on page 76. From the coverage of the folded segments along each base fold line, we find out the overlapping segments. We then remove the segments that overlap with the most other segments until there is no more overlapping.

4.2.2   Generation of Foldable V-Structures

After finalizing the surface segments that can be approximated using v-structures, we proceed to create the actual pop-up. We do this by generating a path of v-structures for each path of potential surface segments. We first generate each v-path such that their angles between the fold lines are equal to the angles on the corresponding input segments. We then adjust the angles of the v-structures to satisfy the foldability condition in Proposition 4.1.

Let us use $\alpha_{1_0}, \beta_{1_0}, \alpha_{2_0}, \beta_{2_0}, ..., \alpha_{n_0}, \beta_{n_0}$ to denote the angles between the edges of the input segments, and $\omega_{\alpha_0}, \omega_{\beta_0}$ to denote their base angles. Each path of v-structures is generated with the initial angles $\omega_\alpha = \omega_{\alpha_0}$, $\omega_\beta = \omega_{\beta_0}$, $\alpha_i = \alpha_{i_0}$ and $\beta_i = \beta_{i_0}$ for all $i \in [1, n]$, where n is the number of pairs of segments forming a potential path.

In order for the v-path to be foldable, according to Proposition 4.1, the angles must satisfy $\omega_\alpha = \sum_1^n \beta_i$ and $\omega_\beta = \sum_1^n \alpha_i$, for all $i \in [1, n]$.

To achieve this, we compute the average amount that each angle ω_α, ω_β, α_i and β_i needs to be adjusted to achieve foldability, $\Delta_\alpha = (\omega_\alpha - \sum \beta_{i_0})/(n+1)$ and $\Delta_\beta = (\omega_\beta - \sum \alpha_{i_0})/(n+1)$. We recompute the angles of the v-structures as $\omega_\alpha = \omega_{\alpha_0} - \Delta_\beta$, $\omega_\beta = \omega_{\beta_0} - \Delta_\alpha$, $\alpha_i = \alpha_{i_0} + \Delta_\alpha$ and

$\beta_i = \beta_{i_0} + \Delta_\beta$. By doing this, the constructed patches form a foldable v-path, while still approximating of the original segments reasonably (Fig. 4.13).

If there are more than one v-paths, they may share some of the patches. However, since each path is distinct, it contains at least one patch that is not shared by any other paths. Hence, we can divide it into shorter paths and adjust the angles on each individual path independently to make it foldable. Fig. 4.14 shows a simple example of such situation. Paths $\mathbb{P}_1 = \{p_1, p_2, p_3, p_4\}$ and $\mathbb{P}_2 = \{p_3, p_4\}$ are overlapping. If we compute the angles for these two paths, α_2, α_3 and β_2 will be constrained by the foldability condition of both paths. However, since path $\mathbb{P}_1$ can be divided into $\{p_1, p_2\}$ and $\{p_3, p_4\}$, we can compute two independent sets of angles, $\{\alpha_3, \beta_2\}$ based on $\{\omega_{\alpha_2}, \omega_{\beta_2}\}$ and $\{\alpha_1, \beta_1\}$ based on $\{\omega_{\alpha_1}, \omega_{\beta_1}\}$.

By generating the paths of v-structures as above, we allow the whole OA to be foldable, while obtaining a reasonable approximation of the input surface segments.
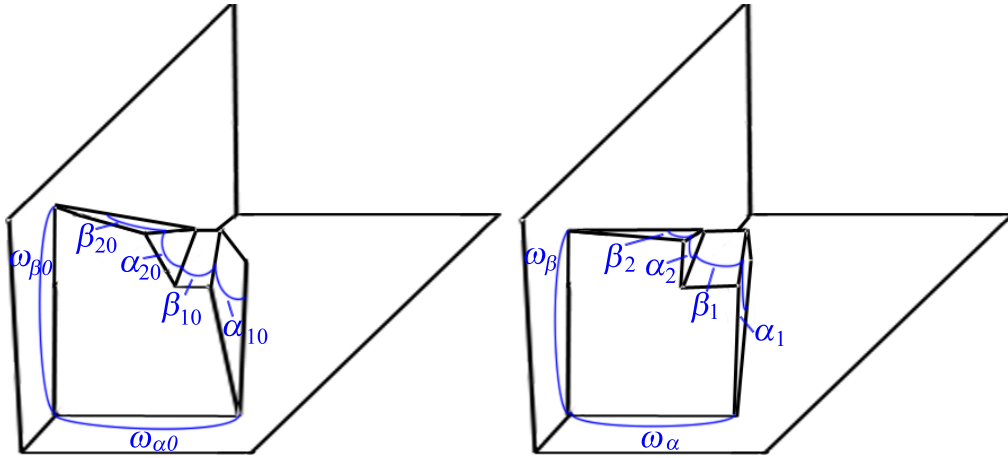
FIGURE 4.13: (Left) A selected path of segments for v-structure generation. (Right) The generated path of v-structures. The angles along the v-path $\{\omega_\alpha, \omega_\beta, \alpha_i, \beta_i\}$ are computed based on the angles along the segment path $\{\omega_{\alpha_0}, \omega_{\beta_0}, \alpha_{i_0}, \beta_{i_0}, ...\}$.

4.2.3 Stabilization of V-Structures

The next step of the v-structure generation is to make them stable. If a v-path has only one structure, it is readily stable. If it contains more than one v-structures, we stabilize it by simply adding double connections to each of the v-structures. Fig. 4.15 shows such a doubly-connect v-structure. We set the angle on the new patch, $\widehat{POP'}$, to range from $1/5$ to $1/3$ of the angle on the original patch, $\widehat{O_\alpha OP}$. In addition, similar to the case of parallel double connections, the width of the new patch, $||PQ||$, is set to $1/6$ of that of the original patch, $||OP||$.

4.3 Results

In practice, that parallel structures and v-structures are not commonly used together in a single OA. From our observation, it is possibly because parallel structures can create nicely uniform shadowing effects. Nevertheless, v-structures are often used to illustrate interesting slanted surfaces.
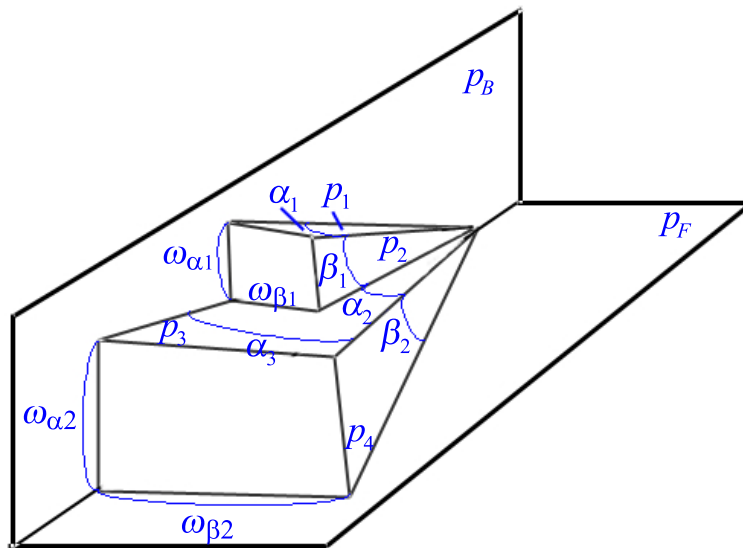
FIGURE 4.14: Overlapping v-paths can be divided into shorter, separate paths, and the angles along each path can be computed independently of those on other paths.
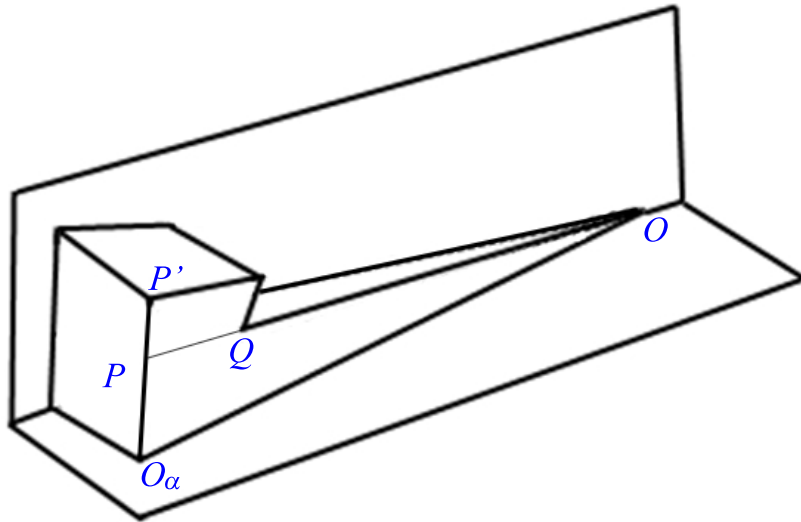
FIGURE 4.15: A doubly-connected v-structure.

In this section, we demonstrate a few results of our method for generating v-structures from input 3D models. As described in section 4.2, we choose to use v-structures only for appropriate planar surfaces that share straight fold lines. In general, given an arbitrary surface, determining whether it should be approximated using parallel structures or v-structures is a challenging problem that will require further comprehensive studies.

We experimented our v-structure generation on input models with
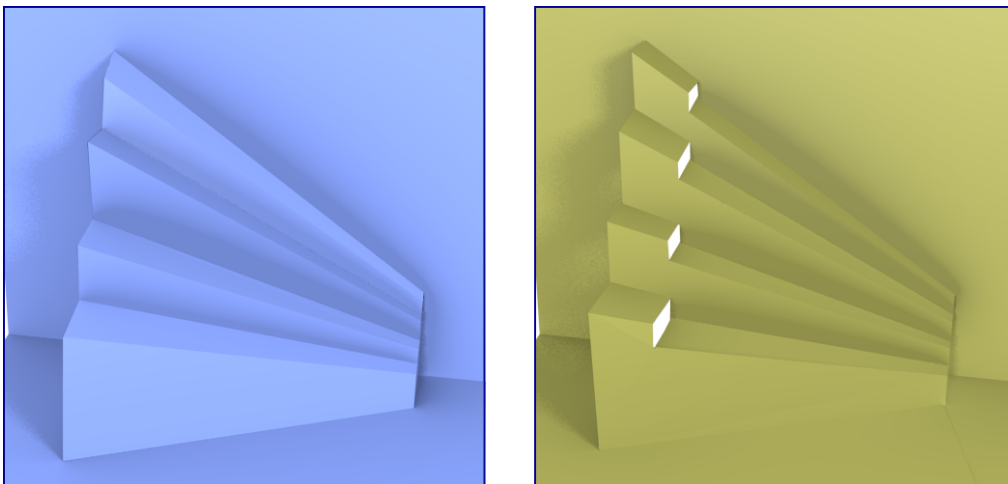
FIGURE 4.16: An arbitrary series of triangular blocks and its corresponding OA.
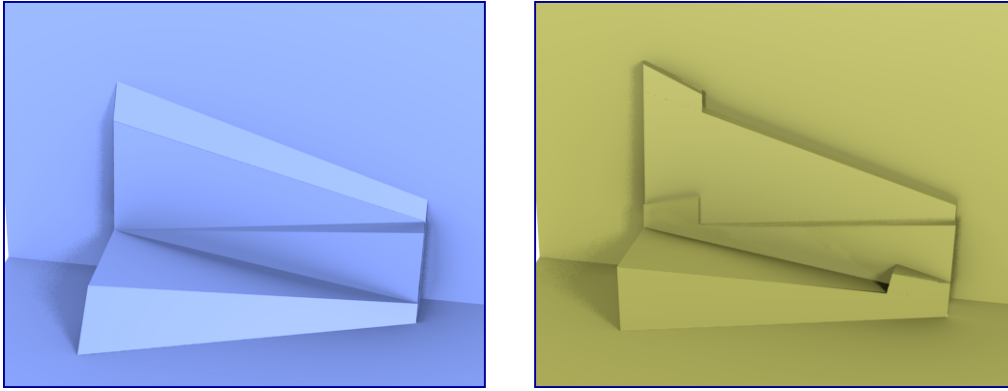
FIGURE 4.17: A series of triangular blocks heading in different directions and its corresponding OA.

various ranges of angles. Figs. 4.16 and 4.17 illustrate two such cases. While the double connections lie on the same side in Fig. 4.16, they sometimes need to be constructed on different sides of the v-path, as shown in Fig. 4.17, due to the limited space between consecutive v-structures.

Note that, although the angles in the input models do not satisfy the foldability condition of non-parallel OAs, we do not need to alter them significantly in our generated structures. In fact, the differences in angles between the input models and the generated OAs are hardly noticeable. This is the result of the simple but effective averaging approach that we use for v-structure generation in section 4.2.2.

Figs. 4.18 and 4.19 demonstrate our generated OAs that resemble interesting shapes. In Fig. 4.18, a v-structure is used to approximate a house model that is intentionally misaligned with the back and floor patches. Note that such model cannot be approximated nicely using parallel structures, as shown in Fig. 3.20 on page 68. In contrast, the slanted house model in Fig. 4.18 can be easily approximated using a simple v-structure.

Fig. 4.19 shows our attempt to create a simple foldable OA that artistically illustrate a pine tree, which is similar to the card in Fig. 4.1 on
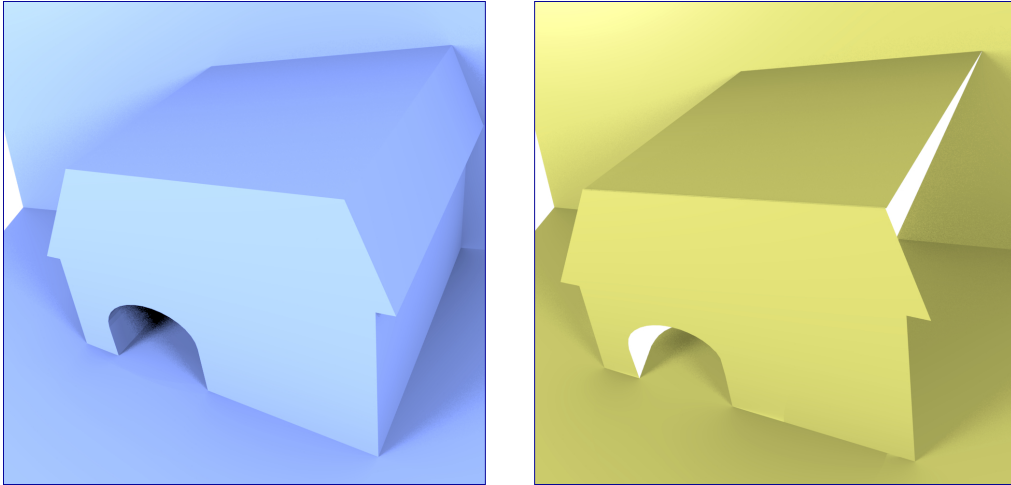
FIGURE 4.18: Non-parallel OAs can be used nicely to illustrate input models that are not aligned to the back and floor bases.

The input model we use is created in Blender software by placing three simple tetrahedra, without the need to constrain any specific angles for them. Our v-structure algorithm then automatically generates the corresponding patches with appropriate angles so that they are fully foldable.
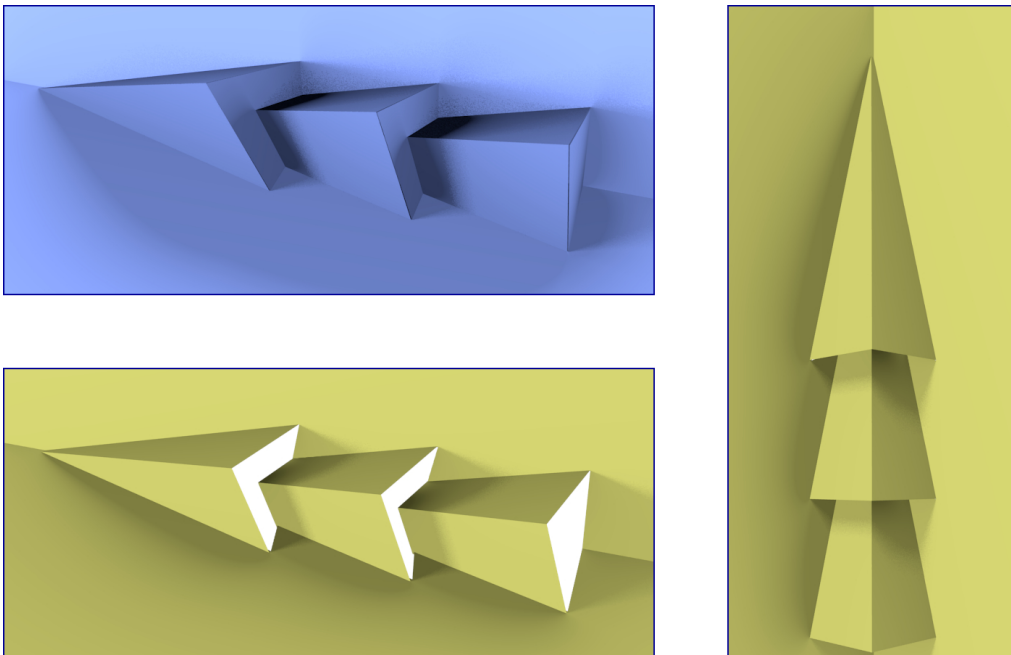
FIGURE 4.19: User-defined triangular blocks with arbitrary angles can be easily converted into a fully foldable OA.
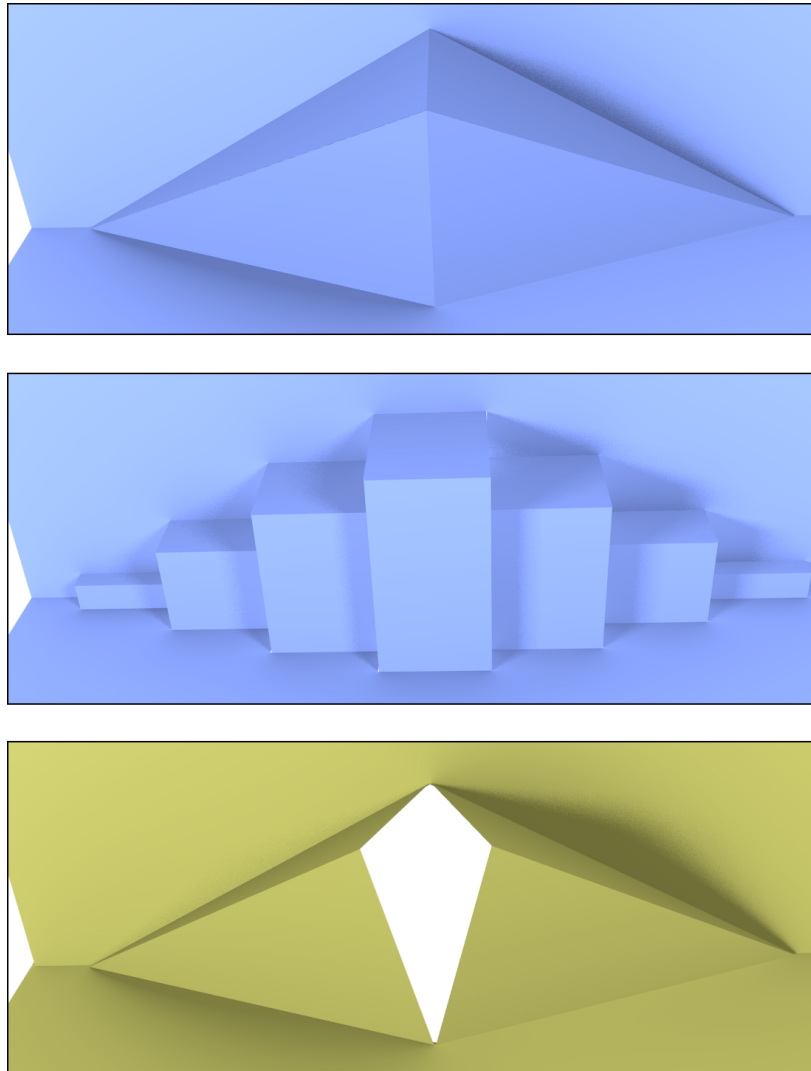
FIGURE 4.20: Non-parallel OA may not always be better than parallel OA for preserving the visual appearance of slanted surfaces.

Note that, while it is relatively easy to create triangular model in 3D modeling software, such as Maya or Blender, it is not trivial to use the correct angles on the faces of the model, so that they can be folded completely when being converted into origamic architecture pop-ups. Our method solves this issue by adjusting each input angle by a reasonable amount so that they satisfy the foldability condition. As shown from Figs. 4.16 to 4.19, the resulting OA structures still approximate the input

models closely.

However, v-structures may not always be the optimal choice for slant-ed surfaces. Fig. 4.20 illustrates a case where parallel structures might possibly be preferred. In this case, the connectivity of the two triangular blocks are not preserved when v-structures are employed. Since only a single piece of paper can be used, the v-structures leave a significant gap between opposite structures when the OA is opened. In parallel structures, the connecting line between two blocks lies on the central patches, and hence no unwanted gap appears during opening and closing.

4.4   Discussion and Conclusion

In this chapter, we have presented a method for designing non-parallel structures in origamic architecture pop-ups, which is also known as v-structures. This method is grounded on our formulated foldability and stability conditions for paths of v-structures. Our simple yet effective algorithm allows creating v-structures as an extended stage in the existing pipeline for OA design. In our extended pipeline, the generation of v-structures comes after the input surface segmentation and before the generation of parallel structures. By selecting appropriate surface segments for approximation using v-structures, we avoid employing over-complicated parallel structures for those segments. Additionally, because the v-structure creation is performed in a separate stage, it does not affect the generated parallel structures later.

Our algorithm first examines the potential surface segments for v-structure generation, then create those structures so that they satisfy our foldability condition, while still approximating the input segments closely. Finally, the generated paths of v-structures are made stable using double connections.

Our stabilizations for parallel structures and for v-structures are strikingly analogous. In both cases, we successfully utilize double connections to stabilize the paths of structures. For v-structures, double connections are defined based on the angles between the fold lines. For parallel structures, double connections are defined based on the distances between the fold lines.

In this chapter, we have proven that doubly-connected v-structures are foldable. From our empirical study, they are also stable during the opening and closing process. However, a formal mathematical proof for the stability of doubly-connected v-structures has yet been achieved. Such proof would strengthen our formulation significantly.

In terms of visual appearance, determining whether v-structures or parallel structures should be used to approximate slanted surfaces with arbitrary fold lines is a challenging question. If v-structures are used, it is not trivial to compute the best angles that are both foldable and closely resemble the non-straight fold lines. In contrast, using parallel structure will lead to an over-complicated and undesired pop-up, as shown in Fig. 3.20. An optimal solution for this problem may require more elaborate shape abstraction techniques.

Chapter 5

Strengthening Origamic Architecture Pop-Ups

In the previous chapters, to facilitate our geometric formulation, we have temporarily assumed that paper has no weight and does not bend. Under that assumption, we were able to construct OA structures that are geometrically both foldable and stable. The latter means when the user holds the two outer patches stationary, no other patches may move.

However, the geometric stability in both our work and [4, 68] does not always hold in practice, when physiscal properties exist. In some cases, most area of a patch is stable, but a small part of it bends because it is too long or not well-supported (Fig. 5.1 (a, c)). In other cases, a horizontal patch may be too big and only supported at the two ends, causing itself to bend down in the middle (Fig. 5.1 (d)).

The instability of patches may not always be because of their weight. In many cases, they may bend due to external forces during the making and holding process (Fig. 5.1 (b)). Hence, such impact also needs to be taken into account in our structural strength analysis.

In computer graphics, much research has been done on the visualization of thin material deformation, notably cloth. A few studies of paper modeling were done based on developable surfaces [12, 57]. These
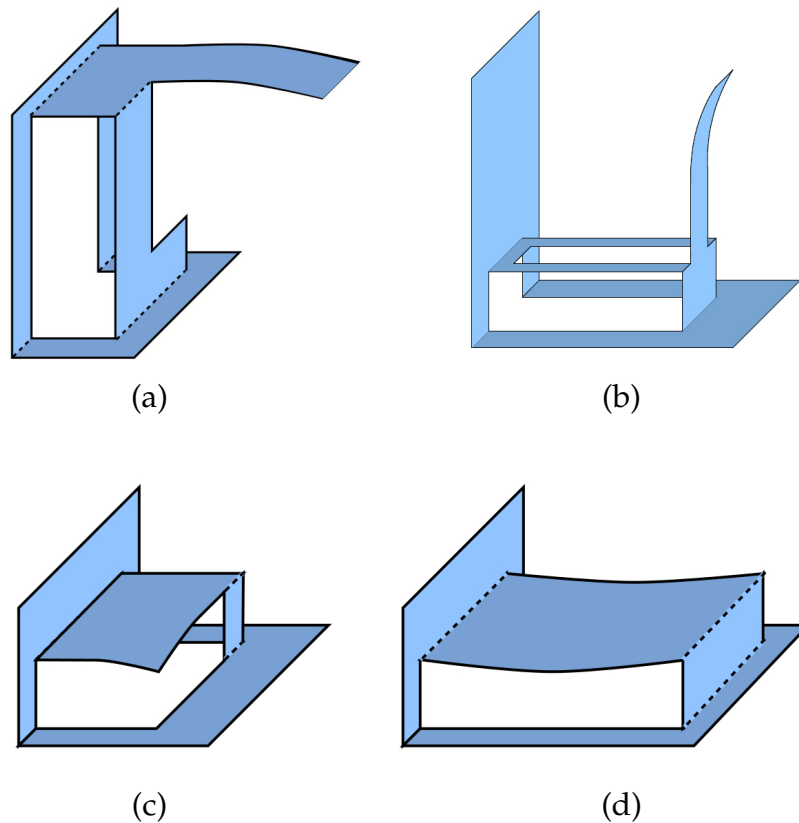
FIGURE 5.1: Bendings in OA structures may occur due to many reasons: (a) Gravity on a long part. (b) External forces during folding and storing. (c) Not being well-supported. (d) Big size.

approaches were mainly for visualization and may not correspond to the actual physical properties of paper, such as mass density and bending stiffness. More recent approaches took into account paper properties, and solved the mesh deformation using Finite Element Method (FEM) [81]. However, this numerical method is computationally expensive. It also involves various types of physical discretization; and hence, is not easy to implement or be readily embed into our design system.

As paper is a thin material, we consider our structural strength analysis a subset of plate analysis, a well-known field in mechanical engineering. In this field, Kirchoff-Love's governing equation [71] is commonly used to compute the plate deflection without the need of carrying

out a full three-dimensional stress analysis as for other types of structures. Although the equation involves differentiation of fourth order, we can find quite accurate results by using Finite Difference Method (FDM). It is a simple method for approximating the solutions of differential equations. FDM is suitable for the scope of our project, as it is very intuitive and easy to implement.

In this study, it is not our goal to produce a highly accurate deformation model of paper pop-ups. We mainly aim to obtain a simple and efficient method to examine whether any parts in an OA paper pop-up may be weak and require fixing. In other words, the method should work efficiently as a post-processing stage of the OA design pipeline. Since the current pipeline takes less than 10 seconds for most input models (section 3.3.2), the method for OA structural strength analysis should be appropriately lightweight. Moreover, we believe that the FDM-based method will be highly reproducible for other interested researchers and developers.

In the following sections, we present our analysis on the physical strength of paper structures using Kirchhoff-Love theory and FDM. From the analysis, we can find out the weak parts and correct them by adding extra supports. This physical analysis is the first of its kind in paper pop-up research.

5.1 Formulations

5.1.1 Governing Equation of Plate Bending

Before analyzing a plate, we need to know how flexible it is. In mechanical engineering, it is called the bending stiffness of the plate, and is computed as

$$D = \frac{Eh^3}{12(1 - \nu^2)} \tag{5.1}$$

where h is the plate thickness, E is the Young's modulus and ν is the Poisson's ratio of the material [21]. Young's modulus measures the stiffness of a material. Poisson's ratio indicates how a material tends to compress (or expand) in one direction when being expanded (or compressed) in the other two directions perpendicular to it.

Kirchhoff-Love theory treats a plate originally as a grid of points on a 2D plane, and computes the deflection at each point on the plate. Let us assume the plate lies in the xy-plane and $w(x, y)$ is the transverse deflection of point (x, y). The theory computes $w(x, y)$ using the following governing differential equation.

$$\frac{\partial^4 w}{\partial x^4} + 2\frac{\partial^4 w}{\partial x^2 \partial y^2} + \frac{\partial^4 w}{\partial y^4} = \frac{p_z(x, y)}{D} \tag{5.2}$$

where $p_z(x, y)$ is the external lateral load at each point.

By using the two-dimensional Laplacian operator

$$\nabla^2(\bullet) = \frac{\partial^2(\bullet)}{\partial x^2} + \frac{\partial^2(\bullet)}{\partial y^2} \tag{5.3}$$

we can rewrite Eq. (5.2) in a more condensed form as

$$\nabla^2 \nabla^2 w(x, y) = \frac{p_z(x, y)}{D} \tag{5.4}$$

In mechanical engineering, when a plate bends significantly, more terms are involved to compute an accurate deformation. However, in our context of paper pop-up, our goal is not to obtain such accurate deformation, but to achieve an approximate amount of bending that may

occur with each patch of paper. From that knowledge, we can determine the patches that may be weak and require more support.

5.1.2 FDM-based Numerical Solution

When a plate has primitive shape, such as round or square, it is possible to find the exact solutions for Eq. 5.4. However, if it has an arbitrary shape, an analytical solution is hard to achieve.

Hence, numerical approaches have been employed to much success. Commonly used methods include Finited difference method (FDM), Finite element method (FEM), Grid-Work Method (GWM) and Boundary Element Method (BEM), to name a few [96].

We choose FDM as its formulations are well-developed and entirely transparent. Unlike FEM, which employs various types of physical discretization, FDM only involves simple mathematical discretization. The number of equations is small, thus they can be conveniently implemented and embedded into our system.

In general, FDM approximates the derivatives using simple linear equations. Consider function $y = f(x)$, where x are discrete points placed equally at the interval $\Delta x = x_{i+1} - x_i$. The derivatives of y at point k can be approximated as follows.

$$
\begin{aligned}
\left(\frac{dy}{dx}\right)_k &\approx \frac{1}{2\Delta x}(y_{k+1} - y_{k-1}) \\
\left(\frac{d^2y}{dx^2}\right)_k &\approx \frac{1}{(\Delta x)^2}(y_{k+1} - 2y_k + y_{k-1}) \\
\left(\frac{d^4y}{dx^4}\right)_k &\approx \frac{1}{(\Delta x)^4}(y_{k+2} - 4y_{k+1} + 6y_k - 4y_{k-1} + y_{k-2})
\end{aligned}
\tag{5.5}
$$

We can also apply FDM on a bivariate function, as in the case of
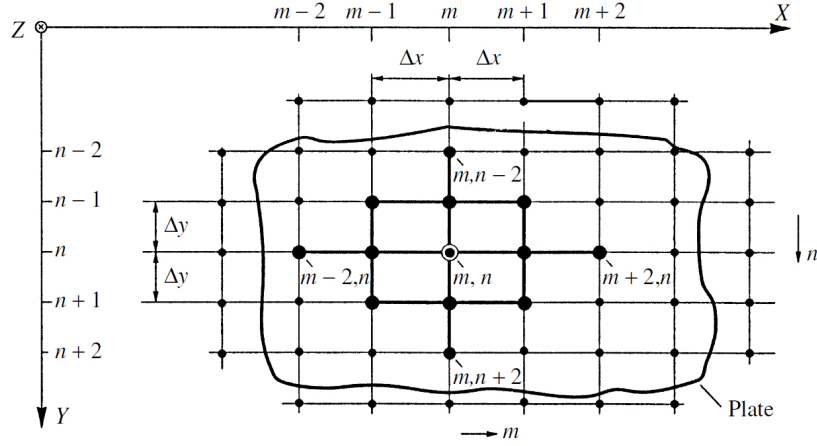
FIGURE 5.2: The setup of points for computing of the plate deflection at (m, n).

plate analysis. We assume the points on the plate are equally spaced and $\Delta x = \Delta y = \delta$ (Fig. 5.2). Then the terms on the left-hand side of Eq. 5.2 at point (m, n) can be approximated using the following equations.

$$
\begin{aligned}
\left(\frac{\partial^4 w}{\partial x^4}\right)_{m,n} &\approx \frac{1}{\delta^4}(w_{m+2,n} - 4w_{m+1,n} + 6w_{m,n} - 4w_{m-1,n} + w_{m-2,n}) \\
\left(\frac{\partial^4 w}{\partial y^4}\right)_{m,n} &\approx \frac{1}{\delta^4}(w_{m,n+2} - 4w_{m,n+1} + 6w_{m,n} - 4w_{m,n-1} + w_{m,n-2})
\end{aligned}
\tag{5.6}
$$

and

$$
\begin{aligned}
\left(\frac{\partial^4 w}{\partial x^2 \partial y^2}\right)_{m,n} &\approx \left\{\frac{\Delta^2}{(\Delta y)^2}\left[\frac{\Delta^2 w}{(\Delta x)^2}\right]\right\}_{m,n} \\
&= \frac{1}{(\Delta y)^2}\left\{\left[\frac{\Delta^2 w}{(\Delta x)^2}\right]_{m,n+1} - 2\left[\frac{\Delta^2 w}{(\Delta x)^2}\right]_{m,n} + \left[\frac{\Delta^2 w}{(\Delta x)^2}\right]_{m,n-1}\right\} \\
&= \frac{1}{\delta^4}(4w_{m,n} - 2(w_{m+1,n} + w_{m-1,n} + w_{m,n+1} + w_{m,n-1}) \\
&\qquad + w_{m+1,n+1} + w_{m+1,n-1} + w_{m-1,n+1} + w_{m-1,n-1})
\end{aligned}
\tag{5.7}
$$

The points involved in approximating the derivatives of $w_{(m,n)}$ are shown in Fig. 5.2. From Eq. 5.6 and 5.7, we can rewrite Eq. 5.4 into the

following form.

$$
\begin{aligned}
\frac{p_z(m,n)}{D} = {} & 20w_{m,n} - 8(w_{m+1,n} + w_{m-1,n} + w_{m,n+1} + w_{m,n-1}) \\
& + 2(w_{m+1,n+1} + w_{m-1,n+1} + w_{m+1,n-1} + w_{m-1,n-1}) \\
& + w_{m+2,n} + w_{m-2,n} + w_{m,n+2} + w_{m,n-2}]
\end{aligned}
\tag{5.8}
$$

This is the main governing equation we use for computing the bending at every point on the paper plate. When we combine these equations for all the points into a linear system, we obtain a very sparse matrix. If the dimension of the plate is $M \times N$, the left-hand side matrix of the system will have dimension $MN \times MN$, but each row only contains at most 13 nonzero coefficients. Hence, we can effectively use available linear system solvers for sparse matrix in our implementation.

For convenient discussion, we also use the following grid format to denote the full form of the governing equation in an intuitive way.
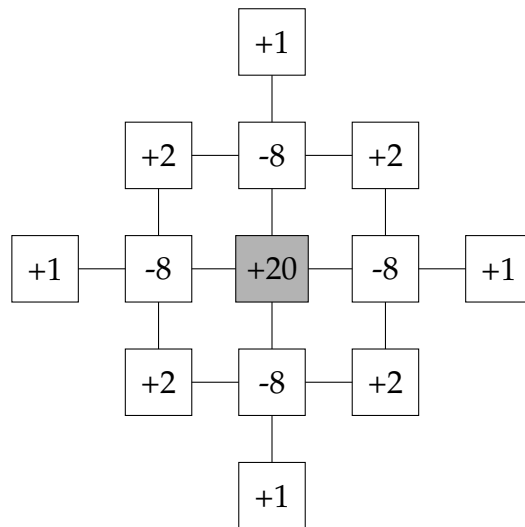
5.1.3 Boundary Conditions

A solution of the discrete governing equation 5.8 must simultaneously

satisfy the equation and the boundary conditions of the plate. Each equation involves 13 points, but these points do not always physically exist. Along the plate boundaries, we must introduce fictitious points outside the plate and express them in terms of the existing ones.

In the scope of paper pop-ups, we consider two types of boundaries. A *fixed edge* is the fold line between two patches, and a *free edge* is along the contour of a cut line. Note that in general structures, we may also have other types of boundaries, such as simple supporting edge, where a plate is placed on top of a supporting point but not fixed to that point.

For each type of boundaries, we need to consider fictitious points outside the plate at distance δ and 2δ from the edge, respectively. Assume the considered edge is parallel to the y-axis, and on the right-hand side of the plate.

On a fixed edge, the bending and its gradient are both zero. Hence, we have the following equations.

$$
\begin{aligned}
w_{m,n} &= 0 \\
\left(\frac{\partial w}{\partial x}\right)_{m,n} &\approx \frac{1}{2\delta}(w_{m+1,n} - w_{m-1,n}) = 0
\end{aligned}
\tag{5.9}
$$

which give the boundary conditions for a fixed edge.

$$
\boxed{
\begin{aligned}
w_{m+1,n} &= w_{m-1,n} \\
w_{m+2,n} &= w_{m-2,n}
\end{aligned}
}
\tag{5.10}
$$

On a free edge, the force and moment about the edge axis have been proven to be zero [96]. They are expressed as

$$
\begin{aligned}
(m_y)_{m,n} &= \left(\frac{\partial^2 w}{\partial y^2} + \nu \frac{\partial^2 w}{\partial x^2}\right)_{m,n} = 0 \\
(v_y)_{m,n} &= \left[\frac{\partial^3 w}{\partial y^3} + (2-\nu)\frac{\partial^3 w}{\partial y \partial x^2}_{m,n}\right] = 0
\end{aligned}
\tag{5.11}
$$

Again, using FDM to approximate the derivatives, we can transform Eq. 5.11 into

$$
\begin{aligned}
(m_y)_{m,n} &\approx -(2+2\nu)w_{m,n} + w_{m,n+1} + w_{m,n-1} + \nu(w_{m+1,n} + w_{m-1,n}) = 0 \\
(v_y)_{m,n} &\approx (6-2\nu)(w_{m,n-1} - w_{m,n+1}) \\
&\quad + (2-\nu)(w_{m+1,n+1} + w_{m-1,w+1} - w_{m-1,n-1} - w_{m+1,n-1}) \\
&\quad - w_{m,n-2} + w_{m,n+2} = 0
\end{aligned}
$$

$$\tag{5.12}$$

From these approximations, we obtain the following linear boundary conditions for a free edge.

$$
\begin{aligned}
w_{m+1,n} &= (2+2\nu)w_{m,n} - w_{m-1,n} - \nu(w_{m,n-1} + w_{m,n+1}) \\
w_{m+2,n} &= (-6\nu^2 + 12\nu + 12)w_{m,n} + (4\nu^2 - 8\nu - 4)(w_{m,n-1} + w_{m,n+1}) \\
&\quad + (4\nu - 12)w_{m-1,n} + (-2\nu + 4)(w_{m-1,n-1} + w_{m-1,n+1}) \\
&\quad + (-\nu^2 + 2\nu)(w_{m,n-2} + w_{m,n+2}) + w_{m-2,n}
\end{aligned}
$$

$$\tag{5.13}$$

From the boundary conditions in Eq. 5.10 and 5.13, we are able to construct the bending equations for every point on the plate, including those along the boundaries.

An arbitrary point may lie on a fixed edge, or a free edge, or it may not lie near any edge. We categorize the position of a point into the

following 11 possible cases.

0. (m, n) has at least distance 2δ from all the edges. In this case, all the involved points in Eq. 5.8 are available, and we do not need to compute the boundary conditions.

1. (m, n) is on a fixed edge.

2. (m, n) is at distance δ from a fixed edge, and is not near any other.

3. (m, n) is at distance δ from two fixed edges.

4. (m, n) is on a free edge, and is not near any other edge.

5. (m, n) is at distance δ from a free edge, and is not near any other.

6. (m, n) is at a corner of two free edges.

7. (m, n) is on a free edge, and at distance δ from another free edge

8. (m, n) is at distance δ from two free edges.

9. (m, n) is on a free edge, and at distance δ from a fixed edge

10. (m, n) is at distance δ from a free edge, and δ from a fixed edge.

An illustration of the points that fall into each of these 11 cases can be seen in the following grid.
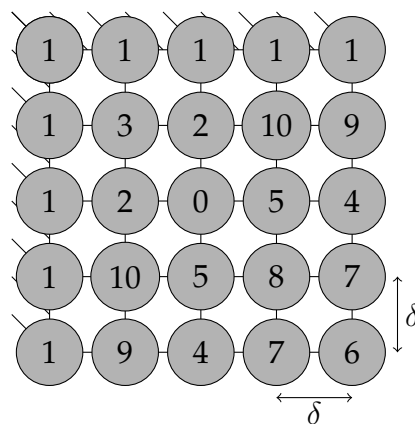
Besides case 0, in which we have the complete governing equation (Eq. 5.8), we need to formulate the equations for the other 10 boundary cases. By using suitable conditions for the fictitious points in each of these cases, we achieve valid equations for all the actual points on the plate. The resulting coefficients of the actual points in each case are as follows.

Case 1: Point (m, n) is on a fixed edge.

The bending at (m, n) is $w_{m,n} = 0$. Hence, no further governing equation is needed.

Case 2: Point (m, n) is at distance δ from a fixed edge but is not near any other edge.

Without loss of generality, we can assume the fixed edge is on the left side of the considered point. From the boundary conditions in Eq. 5.10, we obtain the following governing equation, illustrated in grid form. Note that the bending of points along the fixed edge is zero. Thus, we can ignore their coefficients in the equation.
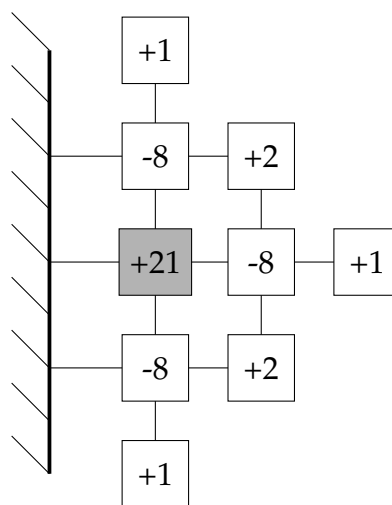
Case 3: Point (m, n) is at distance δ from two fixed edges.

We assume the fixed edges are above and on the left side of the considered point. From Eq. 5.10, we obtain the following governing equation.
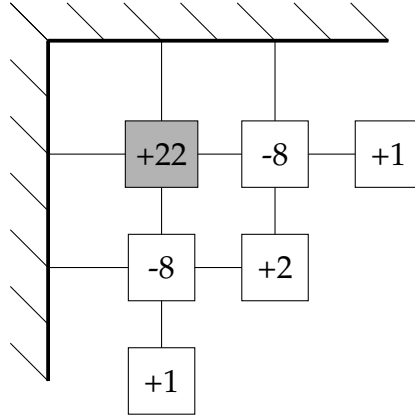
Case 4: Point (m, n) is on a free edge but is not near any other edge.

Assume the considered point is at the bottom of the patch. From Eq. 5.13, we have the following governing equation.
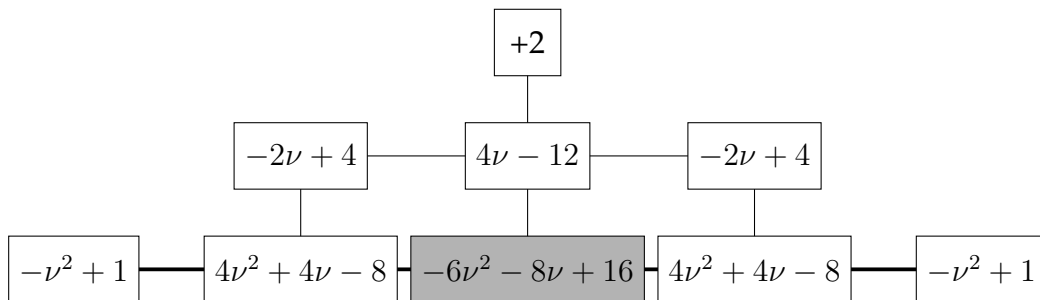
Case 5: Point (m, n) is at distance δ from a free edge but is not near any other edge.

Assume the free edge is below the considered point. From Eq. 5.13, the governing equation becomes
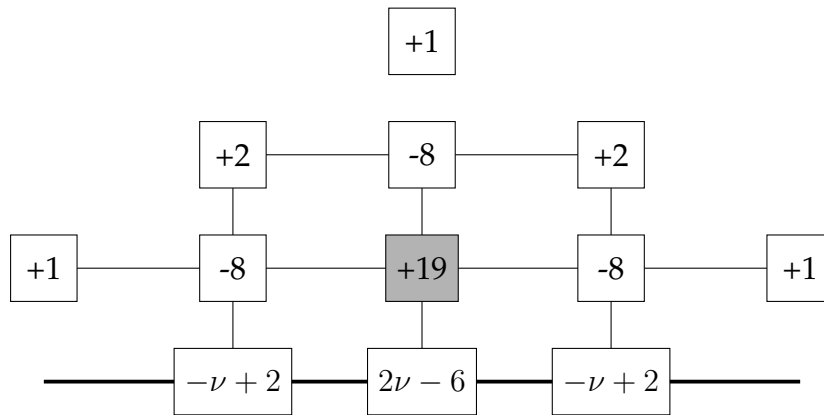
Case 6: Point (m, n) is at the corner of two free edges.

Assume the considered point is at the bottom right corner of the patch. The governing equation becomes
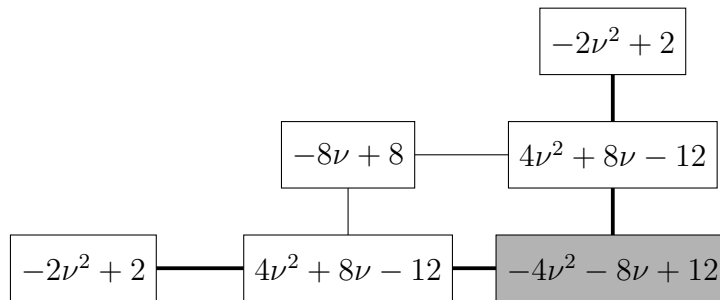
Case 7: Point (m, n) is on a free edge and at distance δ from another free edge.

Assume the considered point is on the right edge and near the bottom edge of the patch. The governing equation becomes
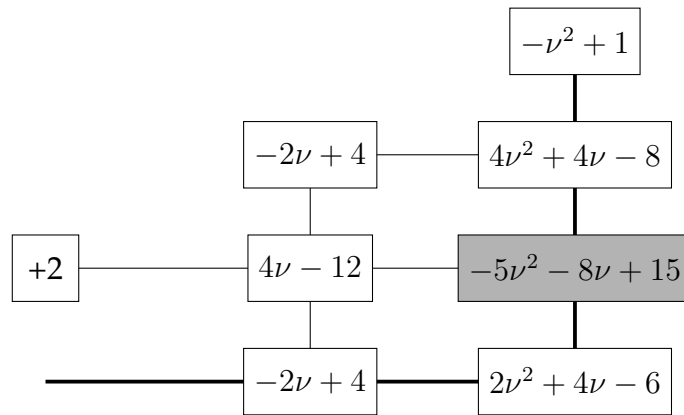
Case 8: Point (m, n) is at distance δ from two free edges.

Assume the considered point is near the bottom right corner of the patch. The governing equation becomes
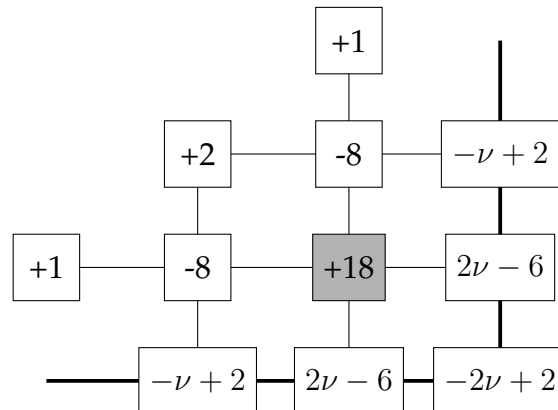
Case 9: Point (m, n) is on a free edge and at distance δ from a fixed edge.

Assume the considered point is near the bottom left corner of the patch. We combine the boundary conditions for both free edge and fixed edge (Eqs. 5.10 and 5.13), which lead to

```
                      ┌────┐
                      │ +2 │
                      └────┘
                         │
┌──────────┐    ┌──────────┐    ┌──────────┐
│ −2ν + 4  │────│ 4ν − 12  │────│ −2ν + 4  │
└──────────┘    └──────────┘    └──────────┘
      │               │               │
┌──────────────┐ ┌──────────────────┐ ┌──────────────┐   ┌──────────┐
│ 4ν² + 4ν − 8 │─│ −7ν² − 8ν + 17    │─│ 4ν² + 4ν − 8 │───│ −ν² + 1  │
└──────────────┘ └──────────────────┘ └──────────────┘   └──────────┘
```
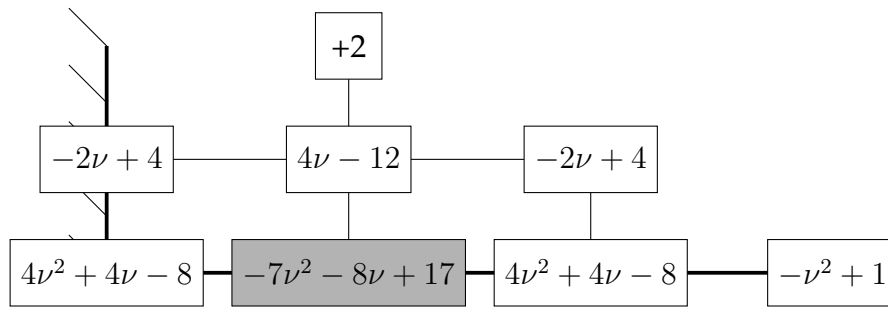
Case 10: The pivotal point is at distance δ from both a free edge and a fixed edge.

Assume the considered point is near the bottom left corner of the patch. The governing equation becomes

```
                  ┌────┐
                  │ +1 │
                  └────┘
                     │
┌────┐    ┌────┐    ┌────┐
│ +2 │────│ -8 │────│ +2 │
└────┘    └────┘    └────┘
   │         │         │
┌────┐   ┌──────┐   ┌────┐   ┌────┐
│ -8 │───│ +20  │───│ -8 │───│ +1 │
└────┘   └──────┘   └────┘   └────┘
   │         │         │
┌────────┐ ┌────────┐ ┌────────┐
│ −ν + 2 │─│ 2ν − 6 │─│ −ν + 2 │────
└────────┘ └────────┘ └────────┘
```
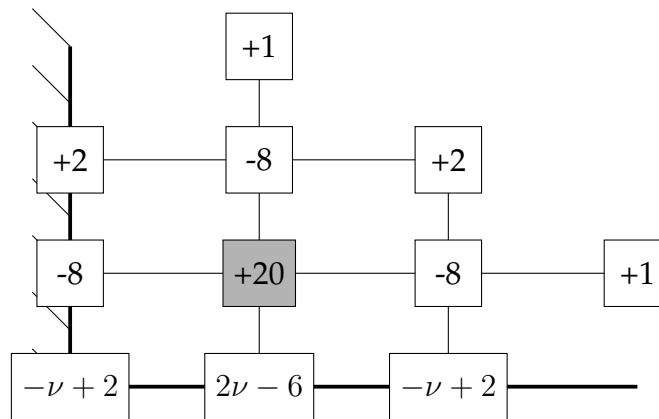
By setting up the equations for all the possible cases of the grid points, we can easily implement the bending of paper patches in our system. Further implementation details are described in the next section.

5.2   Implementation

5.2.1   Bending Approximation for Paper Structures

We assume the generated OA plan has the same dimension as an A4 sheet. For each patch, we set up a mesh of grid to completely cover the patch (Fig. 5.3). We place the grid points regularly at distance $\delta = \Delta x = \Delta y = 5 \times 10^{-3} m$. The physical properties of paper used in our implementation are obtained from the previous literatures. We use card stock density $250 g/m^2$ [3], bending stiffness $D = 5 \times 10^{-2} Nm$ [1] and Poisson's ratio $\nu = 0.3$ [90]. In the governing bending equation (Eq. 5.8 on page 103), the unit for the load at each point is $Newton$ (N), and that for the bending amount is $metre$ (m). We use CSparse library [25] to solve our sparse linear system. All the experimented bendings were computed in real time.
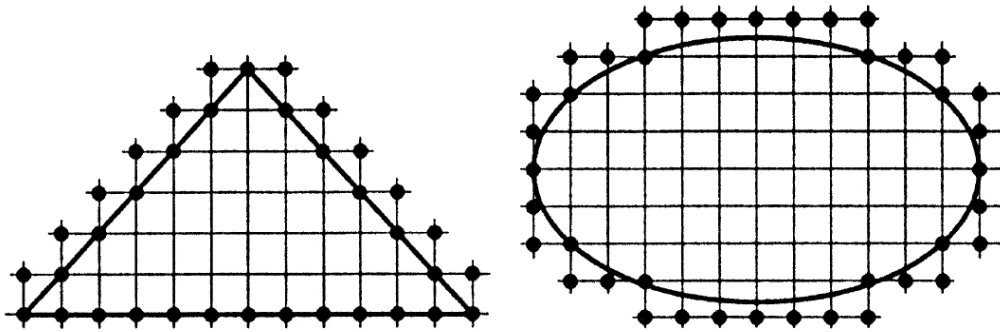
FIGURE 5.3: The mesh of grids is set up to completely cover the shape of the patch.

Currently we only take into account the gravity acting perpendicular to the paper patches. To examine both vertical and horizontal patches, we consider the forces applied on them when the pop-up stands on its floor patch, and when it stands on its back patch. The mass of each patch

is distributed uniformly at every grid point. In the future, we may examine other types of forces, such as rotational forces during the closing and opening process.

5.2.2 Weak Patch Detection and Correction

From the gravity, we compute the possible bending of each patch when the pop-up lies on its floor patch, and when it lies on its back patch. For a pop-up made from an A4 piece of paper, we threshold the bending amount for a weak patch to be at least 0.5cm. If all the points on a patch move less than this amount, it is still considered physically strong.

We also assume that the deflections of the patches are independent. For example, a patch does not bend significantly enough to touch other patches that are originally not adjacent to it. Under this assumption, we iteratively detect the weakest patch, correct it and update the whole structure. The process stops when no more correction is required or can be done.

The correction is achieved by connecting the considered weak part to a strong patch that is connectable to it. This process is similar to the patch connection in Section 3.2.3.2 on page 52, in which we look for the new connection with lowest cost. By doing this, we minimize the changes in the structure when correcting the patches.

As the OA was originally generated with only patches connectable to each other, we can always find a new connection to strengthen a weak patch. Although a global correction method for optimal visual and numerical results is not yet available, our current greedy approach produces acceptable solutions for the tested models, as shown in the next section.

5.3   Results

5.3.1   Comparison with Analytical Solutions

We examine our FDM-based governing equation (Eq. 5.8) by performing it on simple rectangular patches. We then compare our solutions with the analytical solutions for the original differential equation (Eq. 5.4). Figs. 5.4 and 5.5 show the visualizations of the computed bending. In both solutions, we use a patch of size $0.2m \times 0.4m$, with the grid points regularly placed at distance $\Delta x = \Delta y = 10^{-2}m$. The physical properties of the patch are as described in section 5.2.1.
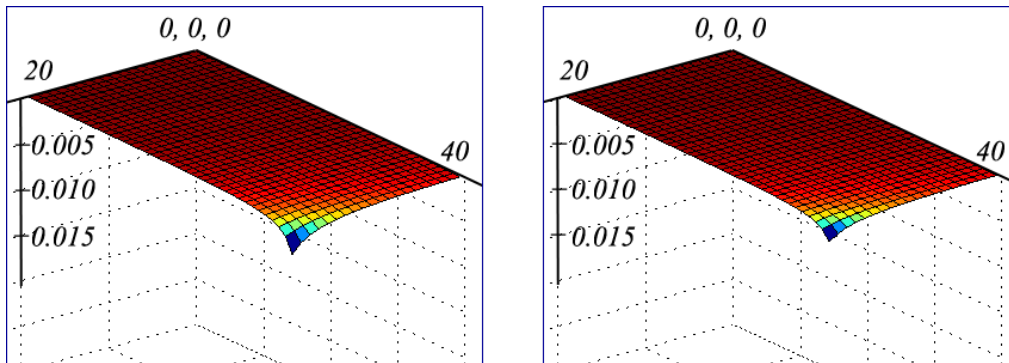
FIGURE 5.4: The computed bending of a patch with two fixed edges and two free edges. Left: Analytical solution of the governing differential equation. Right: Our solution of the FDM-based governing equation.
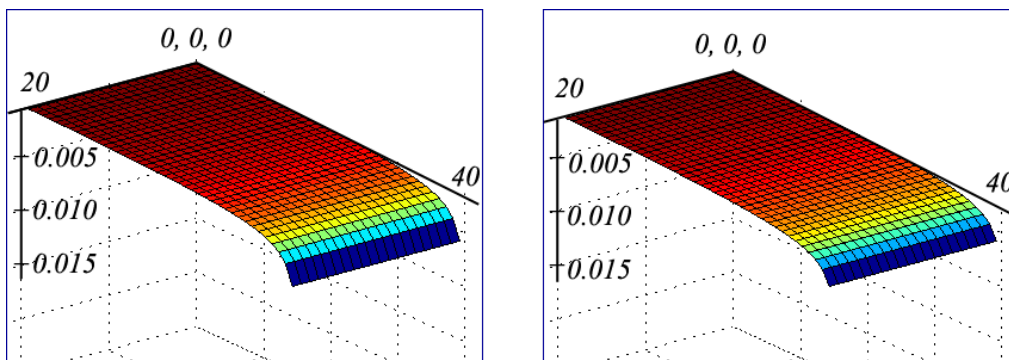
FIGURE 5.5: The computed bending of a patch with one fixed edges and three free edges. Left: Analytical solution of the governing differential equation. Right: Our solution of the FDM-based governing equation.

In the first case, the patch has two fixed edges and two free edges (Fig. 5.4). In the second case, the patch has one fixed edge and three free edges (Fig. 5.5). We compute the average percentage difference from all the grid points of our FDM-based solutions, as compared to the analytical solutions. For the first patch, the percentage difference is 18.22%. For the second patch, the percentage difference is 10.84%. In both cases, the amount of bending computed from the FDM-based solutions is slightly smaller than that from the analytic solutions. However, the positions of the weakest areas are identical in the FDM-based solution and the analytical solution.

The maximal amount of bending of the first patch is $0.36cm$ when using the FDM-based approach, and $0.53cm$ when using the analytical approach. For the second patch, the maximal bending amount for the second patch is $0.64cm$ using the FDM-based approach, and $0.82cm$

(a)   (b)

(c)   (d)
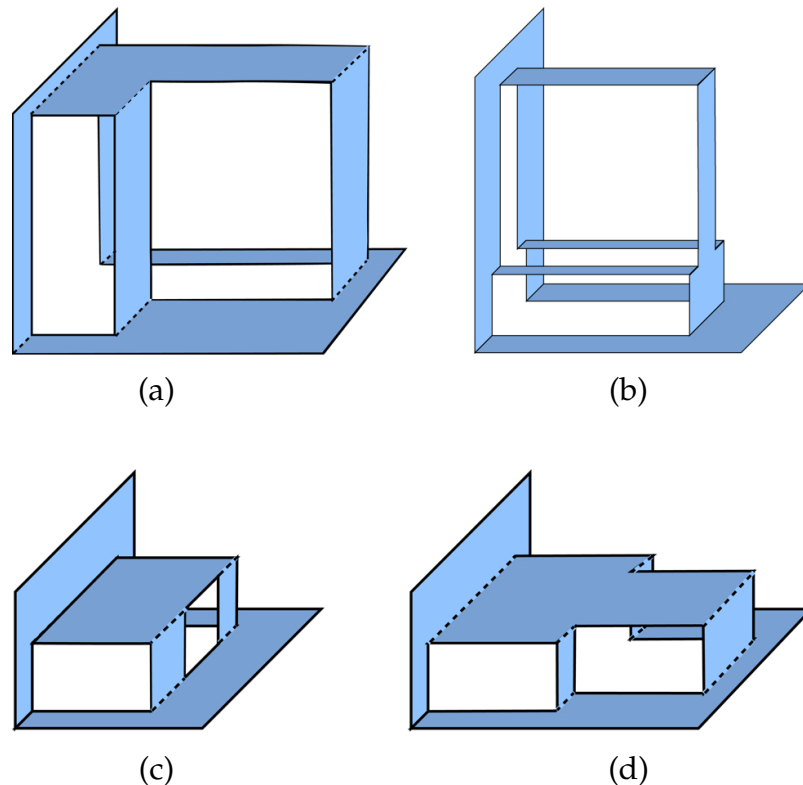
FIGURE 5.6: The weak structures in Fig. 5.1 after being corrected.

(a)	(b)
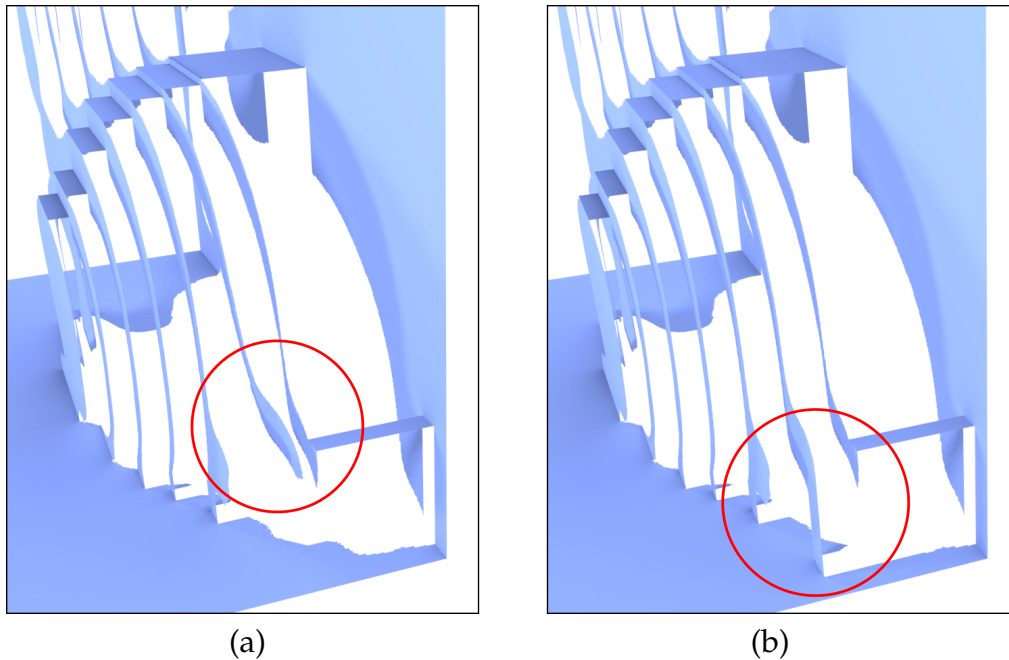
FIGURE 5.7: A patch in the bunny OA is not well-supported (a), and is corrected by extending (b).

when using the analytical approach. This patch is likely to be weak and require extra support along its weakest edge.

5.3.2   OA Structural Strength Analysis and Correction

Although we did not consider physical properties of paper in the previous chapters, our investigation indicates that most of the generated OAs are sufficiently strong. It may be because most patches are supported by at least two other patches, and the input models we use are mostly structurally strong in real life.

Nevertheless, some of the OAs we create contain weak parts that need to be fixed. Figs. 5.1, 5.8, 5.9 and 5.10 show a number of such cases and the corrected designs.

(a)   (b)
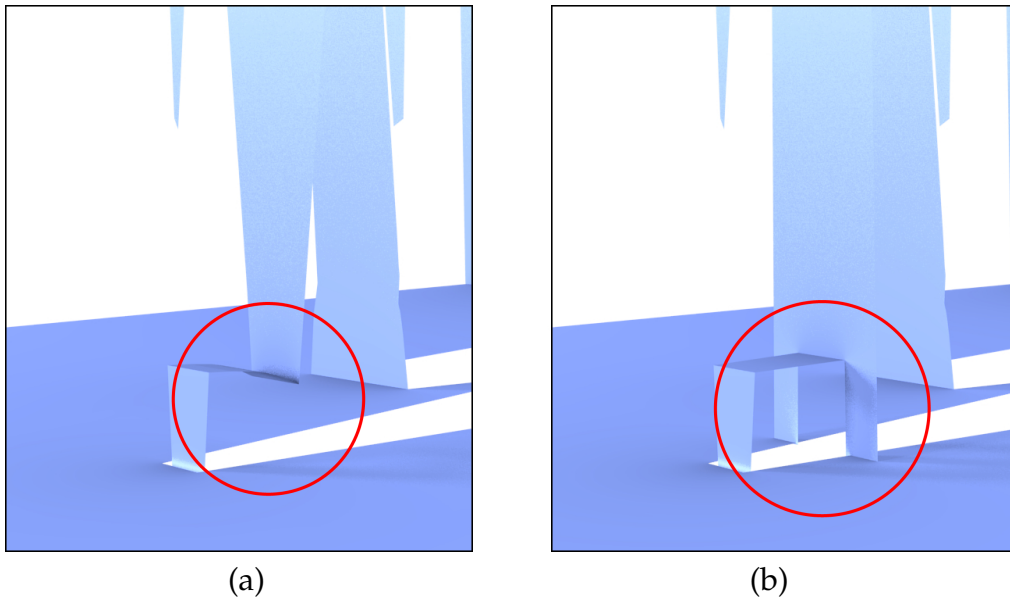
FIGURE 5.8: The trunk of the elephant OA bends down due to the heavy weight (a), and is corrected (b).
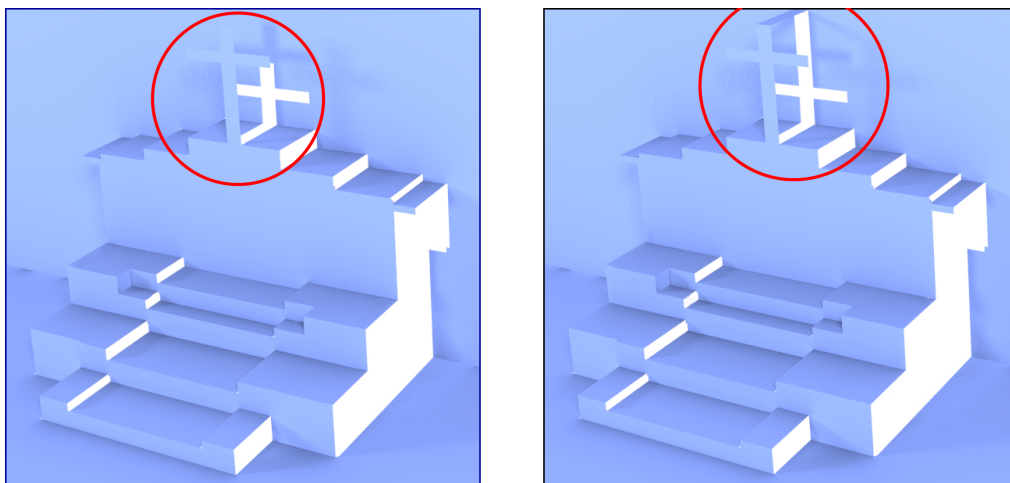
FIGURE 5.9: The cross in the Capitol OA is strengthened.

Note that, in order to make a patch physically strong, we may have to alter its originally desired shape. An example is the trunk of the elephant OA, which has to be widen and connected to the floor patch. An altenative solution in such a situation may be to give the user an option to leave the structure as designed. We can then provide a list of paper

117
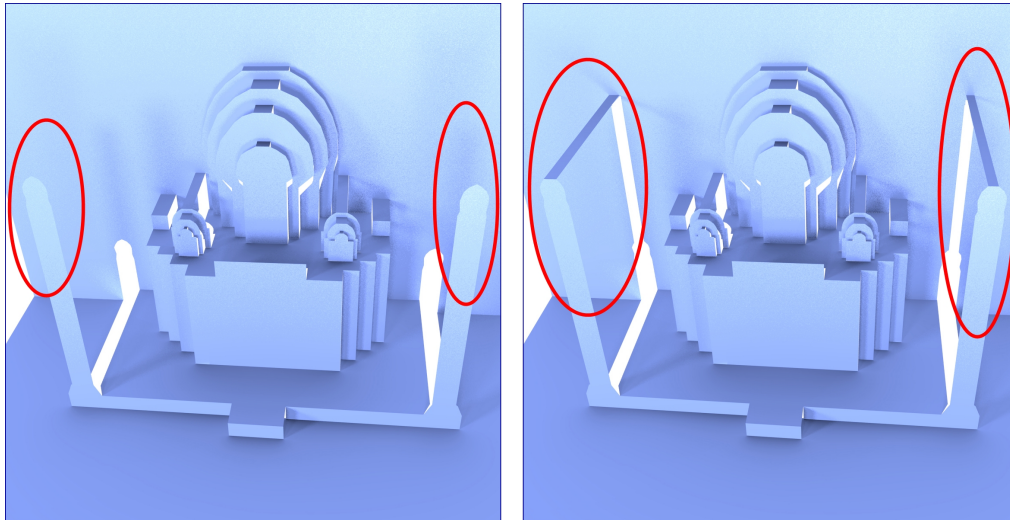
FIGURE 5.10: The cross in the Taj Mahal OA is strengthened.

materials in the system, and allow the user to choose a stronger material for weak pop-ups. In order to do so, more studies on the physical properties of other types of paper will be required.

5.4 Discussion and Conclusion

In this chapter, we have presented a physical strength analysis for paper structures using Kirchhoff-Love theory and FDM discretization. The strength and weakness of each patch is determined by the amount of its bending under gravity when the pop-up lies on the floor patch, and when it lies on the back patch. With its simplicity, the approach is easy to implement, yet effective. Preliminary experiments also show the potential of this approach in analyzing arbitrary structures made of thin materials.

Similar to our stabilization technique in Chapter 3, our physical str-ength analysis can also be readily embedded into other systems for designing paper pop-up, or other types of paper craft. It may also be considered for interactive bending in virtual reality. For instance, a piece

of paper may bend when being pressed or waved by a virtual character. Such object that can respond interactively in a physically-correct manner will be very useful for educational purposes.

Limitations

From our observation in creating pop-ups, the patches seldom bend under longitudinal forces. This may be due to high longitudinal bending stiffness of the card stock material often used for paper pop-ups. Theoretically, longitudinal stiffness is also significantly higher than transverse stiffness that we consider in this work [96]. Thus, to keep the formulation simple, we have yet taken into account longitudinal forces in our work. Nevertheless, when dealing with long thin patches, or more flexible materials (Fig. 5.11), we will need a more elaborate governing equation.
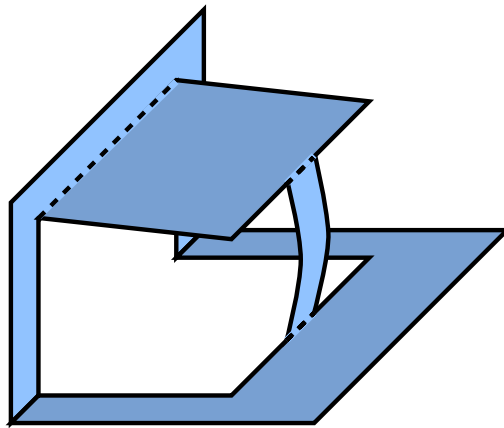
FIGURE 5.11: A long thin patch made from a flexible material is bent due to the weight acting along its longitudial axis.

Our current method detects and corrects one weak patch at a time until all the patches are strong. However, such approach may not be effective for complex structures. For instance, there may be weak patches that can be corrected altogether using a single new connection. Our

method may need to add several connections, and eventually modify the structures more than necessary. To deal with this problem, a global method for structural correction will be needed.

Chapter 6

Conclusion and Future Directions

6.1   Conclusion

Origamic Architecture (OA) not only is a paper art form but also has pratical applications, such as in nano and micro fabrication [30, 47, 107]. As a special type of paper pop-ups, OA has the beauty of using only a single piece of paper, yet inheriting the ability to resemble many structures and daily objects.

Despite its popularity, OA creation requires considerable time and skills. Designing the 2D layout of an OA pop-up is already challenging itself, because it requires careful considerations in both geometric and physical aspects. The design has to pop up fully into a desired shape, while being stable at each opening angle. In addition, it has to be physically strong.

Existing works on computer-aided and automatic OA design are still very limited. In commonly used voxel-based methods, the design process requires high resolution of voxel grid to approximate the input 3D model closely. As a results, the number of cuts and folds caused by the small voxels is significantly high and the voxel-based designs are

hard to use in practice. Even so, the voxels are not able to preserve the meaningful contours on the input surface.

In addition, previous studies only defined a very narrow set of stability conditions for OA structures. As we have examined, those conditions ignore many commonly seen structures, and limit the possible designs significantly.

In this thesis, we have presented a set of geometric formulations and a novel algorithm for automatic OA design. Our comprehensive foldability and stability conditions allow us to utilize an image-based slicing approach for artistically abstracting the input model. We are able to generate foldable and stable pop-up structures that were previously excluded by other algorithms. Visual and quantitative comparisons of results have shown that our algorithm is significantly better than the existing methods in the preservation of contours, surfaces and volume, as well as the ease of actual creation. Our designs have also been shown to resemble those created by real artists.

In addition to the geometric foldability and stability conditions, we formulate a set of linear equations for analyzing the physical strength of the generated OA structures. We utilize Finite Difference Method to discretize Kirchhoff-Love's differential plate equations. By solving the obtained sparse linear system, we simulate the possible bendings in a paper structure in real time. The weak parts can be corrected by adding new supporting connections. Our physical analysis and fixing method is the first of its kind in paper pop-up studies.

All the approaches presented in this thesis, including our novel slicing method, foldability check, stabilization, and physical strength analysis can be easily integrated into other design systems, such as [36, 44], to

name a few. They can help to reduce the manual work for the user, while keeping the pop-ups valid.

6.2 Future Directions

Our study is part of *computational design*, a research area that is becoming more and more active. In this area, our work can be considered *artistic design*, as its goal is to generate results that resemble artists' creations. Another aspect that we plan to study is *functional design*, in which the most important goal is to design objects that function according to user requirements. We aim to continue our research in these two aspects of computational design.

6.2.1 Artistic Design

Paper Pop-Up Our study offers interesting possibilities for future research in general paper pop-up. Theoretically, we have proven the sufficient and necessary condition for foldable OA parallel structures and v-structures, and the sufficient condition for stable parallel structures. However, it is still unknown whether a necessary condition for stable parallel structures is achievable. In addition, the stability condition for v-structures has only been studied empirically, but not been proven mathematically. If a formal proof can be obtained, we will have a stronger theoretical foundation to support a unified framework for both parallel and v-structures.

While origamic architecture only allows a single piece of paper, we may convert it to a general pop-up by adding multiple pieces of paper to preserve the concave surfaces more easily. To do so, we will need to capture a complete shape of the input 3D model by extending our single-view image-based abstraction to multiple views. We have achieve some preliminary results for multi-piece paper pop-ups in [88], [89] (Fig. 6.1).

FIGURE 6.1: The multi-piece paper pop-ups produced by our automatic design systems presented in [88] and [89].

Currently, our abstraction requires as input a 3D model. However, such data may not always be available to all users. We plan to extend our work to allow other types of input representations, for instance drawings and photographs. An OA design system using such inputs will be exciting, and also requires single-view reconstruction techniques. One notable work on single-view pop-up generation is [46]. However, its type of pop-up is still very simple.

Other Paper Art Forms Besides paper pop-up, there are other forms of paper arts such as origami (paper folding) and paper sculpting [22]. For origamic design, although there have been numerous mathematical studies, most of them do not propose an automatic approach, or only generate a complex folding pattern that requires very good skills [97]. For origami learners and beginners, multi-piece origami is a more feasible choice, in which two or more sheets of paper are folded into origamic structures and locked together to form a desired 3D shape. With our experience in origamic architecture and multi-style paper pop-up [88], we believe it is possible to develop an algorithm that searches for a combination of folding patterns to form a multi-piece origami.

Aside from origami, paper sculpting has also been studied recently [72]. However, existing algorithms can only use printed textures to depict subtle details like hair and clothes. In practice, with the flexibility of paper, those details can be abstracted very lively [22] (Fig. 6.2 (a)). We believe an automatic design of detailed and artistic paper sculptures can be achieved by utilizing a multi-view image-domain abstraction method, and studying the effects of physical paper bending for representing different shapes.

6.2.2 Functional Design

Computational design of daily items is becoming more and more

125

a   (b)

FIGURE 6.2: (a) A paper sculpture designed by [22]. (b) Foldable and compact furniture can be designed automatically and 3D-printed in the future.

feasible, especially with the increasing availability of 3D scanning technologies. We are also interested in the automatic design of household and office items, like furniture, that function according to user requirements. The items will be able to perform user-defined mechanical tasks, have a desired appearance and fit in a given space. With the spatial constraints in houses and offices nowadays, it is useful to have foldable and portable items. Similar recent studies, such as [91], do not consider the foldability of the items or their physical balance when the constituent parts are moving. Our earlier geometric formulation for the foldability and stability treats each patch of paper as a rigid plane, and hence, may share similarities with the corresponding geometric study of foldable furniture. However, we will need to take into account the thickness of each part of the furniture, which was not an issue in paper structures. An automatic design system for functional, physically feasible and portable furniture will be of much interest and may open a new horizon for product design (Fig. 6.2 (b)).

Another research direction that requires more elaborate investigation is the computational design of soft and elastic objects, such as clothes. Computational fashion design has not become an active research area,

but will definitely attract much attention. Although cloth simulation has been studied extensively, designing how pieces of cloths can be cut, pleated and sewed together to make nice garments is not easy for most people. It is even more challenging if the garments need to fit the body measurements of a certain person. In this research direction, we can create a system that designs stylish clothes for a person simply from his or her appearance and choices. Such system will require reconstructing human body shape and pose from images or simple measurements, which we have attempted in an earlier project [63, 64]. Moreover, in order to determine the patterns that look good on a person for a specific activity or occasion, it is important to understand the psychological choices in fashion design. This study may benefit from our experience in observing artists choices for paper craft design.

Bibliography

[1] Pulp & paper resources site. http://www.paperonweb.com/, 2010.

[2] Pop-up card books. http://www.evermore.com/oa/books.php3, 2011.

[3] Business card stock. http://standardbusinesscardsize.net/business-card-stock-explained/, 2012.

[4] Z. Abel, E. D. Demaine, M. L. Demaine, S. Eisenstat, A. Lubiw, A. Schulz, D. L. Souvaine, G. Viglietta, and A. Winslow. Universality results for pop-up cards. Preprint, 2012.

[5] E. Agathos, I. Pratikakis, S. Perantonis, N. Sapidis, and P. Azariadis. 3d mesh segmentation methodologies for cad applications. *Computer-Aided Design and Applications*, 4(6):827–842, 2007.

[6] G. Allaire and F. Jouve. Minimum stress optimal design with the level set method. *Engineering Analysis with Boundary Elements*, 32 (11):909918, 2008.

[7] D. Baraff and A. Witkin. Large steps in cloth simulation. In *Proceedings of the 25th annual conference on Computer graphics and interactive techniques*, SIGGRAPH '98, pages 43–54, New York, NY, USA, 1998. ACM.

Bibliography

---

[8] C. Barton. *The Pocket Paper Engineer: How to Make Pop-Ups Step-by-Step*, volume Two volumes. Popular Kinetics Press, 2005-2008.

[9] M. Bataille. *ABC3D*. Roaring Brook Press, 2008.

[10] D. Birmingham. *Pop-Up Design and Paper Mechanics: How to Make Folding Paper Sculpture*. Guild of Master Craftsman, 2011.

[11] P. Block, T. Ciblac, and J. Ochsendorf. Real-time limit analysis of vaulted masonry buildings. *Computers & Structures*, 84(2930):1841–1852, 2006.

[12] P. Bo and W. Wang. Geodesic-controlled developable surfaces for modeling paper bending. In *Computer Graphics Forum*, volume 26, pages 365–374. Wiley Online Library, 2007.

[13] J. Canny. A computational approach to edge detection. *IEEE Trans. Pattern Anal. Mach. Intell.*, 8(6):679–698, June 1986.

[14] L. Carroll and R. Sabuda. *Alice's Adventures in Wonderland: A Pop-up Adaptation*. Little Simon, 2003.

[15] D. A. Carter. *One Red Dot: A Pop-Up Book for Children of All Ages*. Little Simon, 2005.

[16] D. A. Carter and J. Diaz. *Elements of Pop-Up*. Little Simon, 1999.

[17] M. Chatani. *Origamic Architecture of Masahiro Chatani*. Shokokusya, Tokyo, 1984.

[18] M. Chatani. *Pop-Up Origamic Architecture*. Ondorisha Publications, 1985.

[19] M. Chen and K. Tang. A fully geometric approach for developable cloth deformation simulation. *The Visual Computer*, 26(6-8):853–863, 2010.

[20] K.-J. Choi and H.-S. Ko. Stable but responsive cloth. In *ACM SIG-GRAPH 2005 Courses*, SIGGRAPH '05, New York, NY, USA, 2005. ACM.

[21] P. C. Chou. *Elasticity: Tensor, Dyadic, and Engineering Approaches (Dover Civil and Mechanical Engineering)*, volume 1. Dover Publications, 1992.

[22] S. Christopher. Paper Sculptor. http://www.sherchristopher.com/, 2013.

[23] J. Cohen, M. Olano, and D. Manocha. Appearance-preserving simplification. In *Proceedings of the 25th annual conference on Computer graphics and interactive techniques*, SIGGRAPH '98, pages 115–122, New York, NY, USA, 1998. ACM.

[24] CoppeliaRobotics. V-REP. http://www.coppeliarobotics.com/, 2013.

[25] T. A. Davis. *Direct Methods for Sparse Linear Systems (Fundamentals of Algorithms)*. Society for Industrial and Applied Mathematic, 2006.

[26] E. Demaine and J. O'Rourke. *Geometric Folding Algorithms: Linkages, Origami, Polyhedra*. Cambridge University Press, 2007.

[27] E. Eisemann, S. Paris, and F. Durand. A visibility algorithm for converting 3d meshes into editable 2d vector graphics. In *ACM SIGGRAPH 2009 papers*, SIGGRAPH '09, pages 83:1–83:8, New York, NY, USA, 2009. ACM.

[28] E. English and R. Bridson. Animating developable surfaces using nonconforming elements. In *ACM SIGGRAPH 2008 papers*, SIGGRAPH '08, pages 66:1–66:5, New York, NY, USA, 2008. ACM.

[29] J. Feldman and M. Singh. Information along contours and object boundaries. *Psych. Review*, 112:243–252, 2005.

[30] S. M. Felton, M. T. Tolley, B. Shin, C. D. Onal, E. D. Demaine, D. Rus, and R. J. Wood. Self-folding with shape memory composites. *Soft Matter*, 9:7688–7694, 2013.

[31] C. R. Feynman. *Modeling the appearance of cloth*. PhD thesis, Massachusetts Institute of Technology, 1986.

[32] T. Fuse. *Unit Polyhedron Origami*. Japan Publications Trading, 2006.

[33] M. Garland and P. S. Heckbert. Surface simplification using quadric error metrics. In *Proceedings of the 24th annual conference on Computer graphics and interactive techniques*, SIGGRAPH '97, pages 209–216, New York, NY, USA, 1997. ACM Press/Addison-Wesley Publishing Co.

[34] M. Garrido and I. Siliakus. *The Paper Architect: Fold-It-Yourself Buildings and Structures*. Potter Craft, 2009.

[35] M. Gilbert. Ring: A 2d rigid-block analysis program for masonry arch bridges. In *Third International Arch. Bridges Conference*, pages 459–464, 2001.

[36] A. Glassner. Interactive pop-up card design, part 1. In *Computer Graphics and Application*, volume 22, pages 79–86, 2002.

[37] A. Glassner. Interactive pop-up card design, part 2. In *Computer Graphics and Application*, volume 22, pages 74–85, 2002.

[38] R. Goldenthal, D. Harmon, R. Fattal, M. Bercovier, and E. Grinspun. Efficient simulation of inextensible cloth. In *ACM SIGGRAPH 2007 papers*, SIGGRAPH '07, New York, NY, USA, 2007. ACM.

[39] R. C. Gonzalez and R. E. Woods. *Digital Image Processing*. Prentice Hall, 2 edition, 2002.

[40] D. Grant. *The Business of Being an Artist*. Allworth Press, 2010.

[41] T. Hara and K. Sugihara. Computer-aided design of pop-up books with two- dimensional v-fold structures. In *In Proc. 7th Japan Conference on Computational Geometry and Graphs*, 2009.

[42] J. C. Hart, B. Baker, and J. Michaelraj. Structural simulation of tree growth and response. *The Visual Computer*, 19:151–163, 2003.

[43] J. Haslinger and R. A. E. Makinen. *Introduction to Shape Optimization: Theory, Approximation, and Computation*. Society for Industrial and Applied Mathematics, 2003.

[44] S. L. Hendrix and M. A. Eisenberg. Computer-assisted pop-up design for children: computationally enriched paper engineering. *Adv. Technol. Learn.*, 3(2):119–127, April 2006.

[45] M. Hiner. *Paper Engineering for Pop-Up Books and Cards*. Parkwest Pubns, 1986.

[46] D. Hoiem, A. A. Efros, and M. Hebert. Automatic photo pop-up. In *ACM SIGGRAPH 2005 Papers*, pages 577–584, 2005.

[47] E. E. Hui, R. T. Howe, and M. S. Rodgers. Single-step assembly of complex 3-d microstructures. In *The Thirteenth Annual International Conference on Micro Electro Mechanical Systems*, pages 602–607, 2000.

[48] T. Hull. On the mathematics of flat origamis. *Congressus Numerantium*, 100:215–224, 1994.

[49] S. Iizuka, Y. Endo, J. Mitani, Y. Kanamori, and Y. Fukui. An interactive design system for pop-up cards with a physical simulation. *Vis. Comput.*, 27(6-8):605–612, June 2011.

Bibliography

[50] M. Isenburg, P. Lindstrom, S. Gumhold, and J. Snoeyink. Large mesh simplification using processing sequences. In *Proceedings of the 14th IEEE Visualization 2003 (VIS'03)*, VIS '03, pages 61–, Washington, DC, USA, 2003. IEEE Computer Society.

[51] P. Jackson. *The Pop-Up Book: Step-by-Step Instructions for Creating Over 100 Original Paper Projects*. Holt Paperbacks, 1993.

[52] C. Jirasek, P. Prusinkiewicz, and B. Moulia. Integrating biomechanics into developmental plant models expressed using l-systems. In *Plant biomechanics 2000, Proceedings of the 3rd Plant Biomechanics Conference*, pages 615–624. Georg Thieme Verlag, 2000.

[53] J. M. Kaldor, D. L. James, and S. Marschner. Efficient yarn-based cloth with adaptive contact linearization. In *ACM SIGGRAPH 2010 papers*, SIGGRAPH '10, pages 105:1–105:10, New York, NY, USA, 2010. ACM.

[54] E. Kalogerakis, A. Hertzmann, and K. Singh. Learning 3d mesh segmentation and labeling. In *ACM SIGGRAPH 2010 papers*, SIGGRAPH '10, pages 102:1–102:12, New York, NY, USA, 2010. ACM.

[55] L. Kavan, D. Gerszewski, A. W. Bargteil, and P.-P. Sloan. Physics-inspired upsampling for cloth simulation in games. In *ACM SIGGRAPH 2011 papers*, SIGGRAPH '11, pages 93:1–93:10, New York, NY, USA, 2011. ACM.

[56] E. Kenneway. *Complete Origami: An A-Z of Facts and Folds, with Step-by-Step Instructions for Over 100 Projects*. St. Martin's Press, 1987.

[57] M. Kilian, S. Flöry, Z. Chen, N. J. Mitra, A. Sheffer, and H. Pottmann. Developable surfaces with curved creases. In *Advances in Architectural Geometry*, pages 33–36, 2008.

[58] J. Koenderink. *Solid shape*. MIT Press, 1990.

[59] Y.-K. Lai, Q.-Y. Zhou, S.-M. Hu, and R. R. Martin. Feature sensitive mesh segmentation. In *Proceedings of the 2006 ACM symposium on Solid and physical modeling*, SPM '06, pages 17–25, New York, NY, USA, 2006. ACM.

[60] Y.-K. Lai, S.-M. Hu, R. R. Martin, and P. L. Rosin. Rapid and effective segmentation of 3d models using random walks. *Comput. Aided Geom. Des.*, 26(6):665–679, August 2009.

[61] R. J. Lang. *Origami in Action : Paper Toys That Fly, Flap, Gobble, and Inflate*. St. Martin's Griffin, 1997.

[62] L. Lapidus and G. F. Pinder. *Numerical solution of partial differential equations in science and engineering*. Wiley-Interscience, 2011.

[63] S. N. Le, J. Karlekar, and A. C. Fang. Articulated registration of 3d human geometry to x-ray image. In *Image Processing, 2008. ICIP 2008. 15th IEEE International Conference on*, pages 1108–1111, 2008.

[64] S. N. Le, M. K. Lee, S. Banu, and A. C. Fang. Volumetric reconstruction from multi-energy single-view radiography. In *Computer Vision and Pattern Recognition, 2008. CVPR 2008. IEEE Conference on*, pages 1–8, 2008.

[65] S. N. Le, S.-J. Leow, T.-V. Le-Nguyen, C. Ruiz, and K.-L. Low. Surface and contour-preserving origamic architecture paper pop-ups. *IEEE Transactions on Visualization and Computer Graphics*, 20(2):276–288, February 2014.

Bibliography

[66] T.-V. Le, K.-L. Low, C. Ruiz Jr., and S. N. Le. Automatic paper sliceform design from 3d solid models. *IEEE Transactions on Visualization and Computer Graphics*, 19(11):1795–1807, November 2013.

[67] Y. Lee, S. Tor, and E. Soo. Mathematical modelling and simulation of pop-up books. *Computers & Graphics*, 20(1):21–31, 1996.

[68] X.-Y. Li, C.-H. Shen, S.-S. Huang, T. Ju, and S.-M. Hu. Popup: automatic paper architectures from 3d models. In *ACM SIGGRAPH 2010 papers*, SIGGRAPH '10, pages 1–9, 2010.

[69] X.-Y. Li, T. Ju, Y. Gu, and S.-M. Hu. A geometric study of v-style pop-ups: theories and algorithms. In *ACM SIGGRAPH 2011 papers*, SIGGRAPH '11, pages 98:1–98:10, New York, NY, USA, 2011. ACM.

[70] Y. Li, J. Yu, K.-l. Ma, and J. Shi. 3d paper-cut modeling and animation. *Comput. Animat. Virtual Worlds*, 18(4-5):395–403, September 2007.

[71] A. E. H. Love. On the small free vibrations and deformations of elastic shells. *Philosophical trans. of the Royal Society (London)*, serie A(17):491549, 1888.

[72] F. Massarwi, C. Gotsman, and G. Elber. Papercraft models using generalized cylinders. In *Proceedings of the 15th Pacific Conference on Computer Graphics and Applications*, pages 148–157, 2007.

[73] J. Matas, C. Galambos, and J. Kittler. Robust detection of lines using the progressive probabilistic hough transform. *Comput. Vis. Image Underst.*, 78(1):119–137, April 2000.

[74] O. Matias van Kaick and H. Pedrini. A comparative evaluation of metrics for fast mesh simplification. *Computer Graphics Forum*, 25 (2):197–210, 2006.

[75] J. McCrae, K. Singh, and N. J. Mitra. Slices: a shape-proxy based on planar sections. *ACM Trans. Graph.*, 30(6):168:1–168:12, December 2011.

[76] R. Mehra, Q. Zhou, J. Long, A. Sheffer, A. Gooch, and N. J. Mitra. Abstraction of man-made shapes. In *ACM SIGGRAPH Asia 2009 papers*, pages 137:1–137:10, 2009.

[77] J. Mitani and H. Suzuki. Computer aided design for origamic architecture models with polygonal representation. In *Proceedings of the Computer Graphics International*, pages 93–99, 2004.

[78] J. Mitani and H. Suzuki. Making papercraft toys from meshes using strip-based approximate unfolding. *ACM Trans. Graph.*, 23(3): 259–263, August 2004.

[79] A. Montanaro. A concise history of pop-up and movable books. http://www.libraries.rutgers.edu/rulflibs/scua/montanar/p-intro.htm, 2005.

[80] M. Mukerji. *Marvelous Modular Origami*. A K Peters/CRC Press, 2007.

[81] R. Narain, T. Pfaff, and J. F. O'Brien. Folding and crumpling adaptive sheets. *ACM Transactions on Graphics*, 32(4):xxx:1–8, July 2013. Proceedings of ACM SIGGRAPH 2013, Anaheim.

[82] H. N. Ng and R. L. Grimsdale. Computer graphics techniques for modeling cloth. *IEEE Comput. Graph. Appl.*, 16(5):28–41, September 1996.

[83] S. Okamura and T. Igarashi. An assistant interface to design and produce a pop-up card. *International Journal of Creative Interfaces and Computer Graphics*, 1(2):40–50, 2010.

[84] J. O'Rourke. *How to Fold It: The Mathematics of Linkages, Origami, and Polyhedra*. Cambridge University Press, 2011.

[85] D. Pelham. *Trail: Paper Poetry Pop-Up*. Little Simon, 2007.

[86] X. Provot. Deformation constraints in a mass-spring model to describe rigid cloth behaviour. In *Graphics interface*, pages 147–147. Canadian Information Processing Society, 1995.

[87] E. G. Rubin. A history of pop-up and movable books: 700 years of paper engineering.
http://www.youtube.com/watch?v=iDJJOaZ1myM, November 2010. Public lecture.

[88] C. J. Ruiz, S. N. Le, and K.-L. Low. Generating multi-style paper pop-up designs using 3d primitive fitting. In *ACM SIGGRAPH Asia Technical Briefs*, SA '13, pages 4:1–4:4, 2013.

[89] C. J. Ruiz, S. N. Le, J. Yu, and K.-L. Low. Multi-style paper pop-up designs from 3d models. *Computer Graphics Forum*, 3(2):–, 2014.

[90] K. Schulgasser. The in-plane poisson ratio of paper. *Fibre Science and Technology*, 19(4):297–309, 1983.

[91] Y. Schwartzburg and M. Pauly. Fabrication-aware design with intersecting planar pieces. *Computer Graphics Forum*, 32(2pt3):317–326, 2013.

[92] A. Shamir. A survey on mesh segmentation techniques. *Computer Graphics Forum*, 27(6):1539–1556, 2008.

[93] I. Shatz, A. Tal, and G. Leifman. Paper craft models from meshes. *Vis. Comput.*, 22(9):825–834, September 2006.

[94] O. Stava, J. Vanek, B. Benes, N. Carr, and R. Mech. Stress relief: Improving structural strength of 3d printable objects paper abstract. In *In ACM SIGGRAPH 2012 papers*, 2012.

[95] K. A. Stevens. The visual interpretation of surface contours. *Artificial Intelligence*, 17(13):47–73, 1981.

[96] R. Szilard. *Theories and Applications of Plate Analysis: Classical Numerical and Engineering Methods*. Wiley, 2004.

[97] T. Tachi. Origamizing polyhedral surfaces. *IEEE Transactions on Visualization and Computer Graphics*, 16(2):298–311, March 2010.

[98] TamaSoftware. Pepakura designer.
http://www.tamasoft.co.jp/pepakura-en/, 2007.

[99] A. Telea and A. Jalba. Voxel-based assessment of printability of 3d shapes. In *Proceedings of the 10th international conference on Mathematical morphology and its applications to image and signal processing*, ISMM'11, pages 393–404, Berlin, Heidelberg, 2011. Springer-Verlag.

[100] D. Terzopoulos, J. Platt, A. Barr, and K. Fleischer. Elastically deformable models. In *ACM Siggraph Computer Graphics*, volume 21, pages 205–214. ACM, 1987.

[101] B. Thomaszewski, M. Wacker, and W. Straß er. A consistent bending model for cloth simulation with corotational subdivision finite elements. In *Proceedings of the 2006 ACM SIGGRAPH/Eurographics symposium on Computer animation*, SCA '06, pages 107–116, Aire-la-Ville, Switzerland, Switzerland, 2006. Eurographics Association.

[102] J. Todd and F. Reichel. Visual perception of smoothly curved surfaces from double-projected contour patterns. *J. of Exp. Psych.: Human Percep. and Perform.*, 16:665–674, 1990.

[103] R. Uehara and S. Teramoto. The complexity of a pop-up book. In *In Proc. 18th Canadian Conference on Computational Geometry*, 2006.

[104] P. Volino, N. Magnenat-Thalmann, and F. Faure. A simple approach to nonlinear tensile stiffness for accurate cloth simulation. *ACM Transactions on Graphics*, 28(4):105:1–105:16, 2009.

[105] J. Weil. The synthesis of cloth objects. In *Proceedings of the 13th annual conference on Computer graphics and interactive techniques*, SIGGRAPH '86, pages 49–54, New York, NY, USA, 1986. ACM.

[106] E. Whiting, J. Ochsendorf, and F. Durand. Procedural modeling of structurally-sound masonry buildings. In *ACM SIGGRAPH Asia 2009 papers*, SIGGRAPH Asia '09, pages 112:1–112:9, New York, NY, USA, 2009. ACM.

[107] J. Whitney, P. Sreetharan, K. Ma, and R. Wood. Pop-up book mems. *Journal of Micromechanics and Microengineering*, 21(11):115021, 2011.

[108] J. Xu, C. S. Kaplan, and X. Mi. Computer-generated papercutting. In *Proceedings of the 15th Pacific Conference on Computer Graphics and Applications*, pages 343–350. IEEE Computer Society, 2007.